High scale mixing relations as a natural explanation for large neutrino mixing

Gauhar Abbas,[1,*] Mehran Zahiri Abyaneh,[1,†] Aritra Biswas,[2,‡] Saurabh Gupta,[3,§] Monalisa Patra,[4,¶] G. Rajasekaran,[2,5] and Rahul Srivastava[2,**]

[1] *IFIC, Universitat de València – CSIC, Apt. Correus 22085, E-46071 València, Spain*

[2] *The Institute of Mathematical Sciences, Chennai 600 113, India*

[3] *Instituto de Física, Universidade de São Paulo, C. Postal 66318, 05314-970 São Paulo, Brazil*

[4] *Physik-Institut, Universität Zürich, CH-8057 Zürich, Switzerland*

[5] *Chennai Mathematical Institute, Siruseri 603 103, India*

The origin of small mixing among the quarks and a large mixing among the neutrinos has been an open question in particle physics. In order to answer this question, we postulate general relations among the quarks and the leptonic mixing angles at a high scale, which could be the scale of Grand Unified Theories. The central idea of these relations is that the quark and the leptonic mixing angles can be unified at some high scale either due to some quark-lepton symmetry or some other underlying mechanism and as a consequence, the mixing angles of the leptonic sector are proportional to that of the quark sector. We investigate the phenomenology of the possible relations where the leptonic mixing angles are proportional to the quark mixing angles at the unification scale by taking into account the latest experimental constraints from the neutrino sector. These relations are able to explain the pattern of leptonic mixing at the low scale and thereby hint that these relations could be possible signatures of a quark-lepton symmetry or some other underlying quark-lepton mixing unification mechanism at some high scale linked to Grand Unified Theories.

PACS numbers: 14.60.Pq, 11.10.Hi, 11.30.Hv, 12.15.Lk

*Electronic address: Gauhar.Abbas@ific.uv.es

†Electronic address: Mehran.Za@ific.uv.es

I. INTRODUCTION

The quark mixing matrix, V_{CKM}, parametrizes the misalignment in the diagonalisation of the *up* and *down* type quark mass matrices. It is well known that V_{CKM} is almost close to a unit matrix. This implies that the quark mixing angles are small. On the other hand, analogous misalignment in the leptonic sector is encoded in the neutrino mixing matrix, U_{PMNS}. It turns out that U_{PMNS} is not close to a unit matrix. The mixing angles in the neutrino sector are large except θ_{13} [1–3]. The origin of small mixing among quarks and a large mixing in the neutrino sector poses an intriguing open question.

Among many approaches to explain the mixing pattern of the leptons, the assumption of family or flavor symmetries is a popular one. These symmetries differentiate among the members of different families and are usually discrete, finite and non-abelian, for reviews see Refs. [4, 5]. This approach has been intensively used to study the mixing in the leptonic sector [6–9]. In addition to the leptonic mixing, there are also considerable efforts to understand the quark mixing through family symmetries [10–12]. The family symmetries can also be a built-in characteristic of the Grand Unified Theories (GUT) [13].

The quark-lepton unification is one of the most attractive features of the GUT theories [14–16]. The GUT symmetry group contains quarks and leptons in a joint representation. The weak interaction properties of the quarks and the leptons therefore get correlated. Hence it is possible in these theories, to derive the origin of the small and the large mixing in the quark and the lepton sectors respectively, along with any relation between them, if it exists.

There are also reasons to speculate about the quark-lepton unification even on the experimental side. The so-called quark-lepton complementarity (QLC) relation [17, 18] between the leptonic mixing angle θ_{12} and the Cabibbo angle θ_C

$$\theta_{12} + \theta_C \approx \frac{\pi}{4}, \tag{1}$$

can be a footprint of a high scale quark-lepton unification [17–21]. Another interesting observation is due to the recent non-zero measurement of leptonic mixing angle θ_{13} [22–26]

[‡]Electronic address: aritrab@imsc.res.in
[§]Electronic address: saurabh@if.usp.br
[¶]Electronic address: monalisa@physik.uzh.ch
[**]Electronic address: rahuls@imsc.res.in

which is

$$\theta_{13} \approx \frac{\theta_C}{\sqrt{2}}. \tag{2}$$

This relation also hints a possible link between the quark and leptonic mixing, and it can be an artifact of some high scale quark-lepton symmetry in an underlying GUT theory [27].

Therefore, the present state of the measured leptonic mixing angles provide the theoretical motivation for a common origin of the quark and leptonic mixing at some high scale. In fact, the idea that the quark and lepton mixing can be unified at some high scale, referred to as "high scale mixing unification" (HSMU) hypothesis, was first proposed in Ref. [28–31]. In recent studies [32–34] it has been shown that HSMU hypothesis 'naturally' leads to nonzero and a small value for the leptonic mixing angle θ_{13} and predicts a non-maximal θ_{23} (cf. [32, 34] for details). This hypothesis has been studied in the context of Dirac neutrinos as well (cf. [35] for details). The central idea of this hypothesis is that the quark mixing angles become identical to that of the leptons at some high scale (referred to as the unification scale) which is typically taken as GUT scale (cf. [32, 33, 35] for details). In other words, at the unification scale

$$\theta_{12} = \theta^q_{12}, \quad \theta_{13} = \theta^q_{13}, \quad \theta_{23} = \theta^q_{23}, \tag{3}$$

where θ_{ij} (with $i, j = 1, 2, 3$) are leptonic mixing angles and θ^q_{ij} are the quark mixing angles. This hypothesis nicely explains the pattern of mixing in the neutrino sector including the recent observation of nonzero and a small value of θ_{13} [22–26]. The large leptonic mixing angles at the low scale are obtained through the renormalization group (RG) evolution of the corresponding mixing parameters from the unification scale to the low scale.

The implementation of the HSMU hypothesis requires the minimum supersymmetric standard model (MSSM) as an extension of the standard model (SM). The working of the HSMU hypothesis is as follows. We first evolve the quark mixing angles from the low scale (mass of the Z boson) to the supersymmetry (SUSY) breaking scale using the SM RG equations. After that, from the SUSY breaking scale to the unification scale, evolution of quark mixing angles is governed by the MSSM RG equations. In the next step, the quark mixing angles at the unification scale, are put equal to that of the neutrinos following the HSMU hypothesis. The leptonic mixing parameters are then run from the unification scale to the SUSY breaking scale using the MSSM RG equations. From the SUSY breaking scale to the low scale, mixing parameters are evolved through the SM RG equations.

In addition to SUSY, we also need a large $\tan\beta$ to realize the HSMU hypothesis [32, 33]. The only free parameters during the top-down running of the leptonic mixing parameters are masses of the three light neutrinos. They are chosen at the unification scale in such a manner that we recover all the mixing parameters at the low scale within the 3σ limit of the global fit. It turns out that the chosen masses of neutrinos must be quasi-degenerate (QD) and normal hierarchical [32, 33]

In this work, inspired by the HSMU hypothesis, we postulate the most general relations among the quark and the leptonic mixing angles at the unification scale. In a compactified form the most general relation among the leptonic and the quark mixing angles within the same generations is as following

$$\theta_{12} = \alpha_1^{k_1}\ \theta_{12}^q, \quad \theta_{13} = \alpha_2^{k_2}\ \theta_{13}^q, \quad \theta_{23} = \alpha_3^{k_3}\theta_{23}^q. \tag{4}$$

where k_i, with $i = (1, 2, 3)$ are real exponents. We refer to this relation as the "high scale mixing relation" (HSMR). We have chosen (k_1, k_2, k_3) to be $(1, 1, 1)$ for the simplicity of our analysis. The relations within the same generations are the simplest generalization of the HSMU hypothesis. In principle, we can also construct the most general HSMR relations among different generations completely independent of the HSMU hypothesis. The analysis of these relations is beyond the scope of this work and could be studied elsewhere.

There will be different possibilities depending on the relations among the proportionality factors. We firstly list below the different possible cases with the maximum and the minimum allowed values of the three independent proportionality factors α_i,

$$\textbf{Case A}: \quad \theta_{12} = \alpha_1^{max}\ \theta_{12}^q, \quad \theta_{13} = \alpha_2^{max}\ \theta_{13}^q, \quad \theta_{23} = \alpha_3^{max}\ \theta_{23}^q, \tag{5}$$

$$\textbf{Case B}: \quad \theta_{12} = \alpha_1^{max}\ \theta_{12}^q, \quad \theta_{13} = \alpha_2^{max}\ \theta_{13}^q, \quad \theta_{23} = \alpha_3^{min}\ \theta_{23}^q, \tag{6}$$

$$\textbf{Case C}: \quad \theta_{12} = \alpha_1^{max}\ \theta_{12}^q, \quad \theta_{13} = \alpha_2^{min}\ \theta_{13}^q, \quad \theta_{23} = \alpha_3^{max}\ \theta_{23}^q, \tag{7}$$

$$\textbf{Case D}: \quad \theta_{12} = \alpha_1^{max}\ \theta_{12}^q, \quad \theta_{13} = \alpha_2^{min}\ \theta_{13}^q, \quad \theta_{23} = \alpha_3^{min}\ \theta_{23}^q, \tag{8}$$

$$\textbf{Case E}: \quad \theta_{12} = \alpha_1^{min}\ \theta_{12}^q, \quad \theta_{13} = \alpha_2^{max}\ \theta_{13}^q, \quad \theta_{23} = \alpha_3^{max}\ \theta_{23}^q, \tag{9}$$

$$\textbf{Case F}: \quad \theta_{12} = \alpha_1^{min}\ \theta_{12}^q, \quad \theta_{13} = \alpha_2^{max}\ \theta_{13}^q, \quad \theta_{23} = \alpha_1^{min}\ \theta_{23}^q, \tag{10}$$

$$\textbf{Case G}: \quad \theta_{12} = \alpha_1^{min}\ \theta_{12}^q, \quad \theta_{13} = \alpha_2^{min}\ \theta_{13}^q, \quad \theta_{23} = \alpha_3^{max}\ \theta_{23}^q, \tag{11}$$

$$\textbf{Case H}: \quad \theta_{12} = \alpha_1^{min}\ \theta_{12}^q, \quad \theta_{13} = \alpha_2^{min}\ \theta_{13}^q, \quad \theta_{23} = \alpha_3^{min}\ \theta_{23}^q. \tag{12}$$

In this work, we have presented our results for the maximum and minimum allowed values

of α_i for all the above cases, Eqs. (5-12). We then move on to scenarios, assuming relations among the α_i's. There can be more general HSMR where two proportionality constants can be identical and the third one is different. However we will discuss in this work more simplified scenerios, where the three proportionality constants are equal.

$$\theta_{12} = \alpha^{k_1}\ \theta^q_{12}, \quad \theta_{13} = \alpha^{k_2}\ \theta^q_{13}, \quad \theta_{23} = \alpha^{k_3}\theta^q_{23}. \tag{13}$$

As explained before we have restricted to values of k_i as either 0 or 1. We note that the value $(k_1, k_2, k_3) = (0, 0, 0)$ will reduce HSMR to HSMU hypothesis making Eq. (3) a specific form of HSMR, Eq. (13). We present below the seven different possible cases, where the quark mixing angles are assumed to be proportional to the corresponding leptonic mixing angles.

$$\textbf{Case 1}: \quad \theta_{12} = \alpha\ \theta^q_{12}, \quad \theta_{13} = \theta^q_{13}, \quad \theta_{23} = \theta^q_{23}, \tag{14}$$

$$\textbf{Case 2}: \quad \theta_{12} = \theta^q_{12}, \quad \theta_{13} = \alpha\ \theta^q_{13}, \quad \theta_{23} = \theta^q_{23}, \tag{15}$$

$$\textbf{Case 3}: \quad \theta_{12} = \theta^q_{12}, \quad \theta_{13} = \theta^q_{13}, \quad \theta_{23} = \alpha\ \theta^q_{23}, \tag{16}$$

$$\textbf{Case 4}: \quad \theta_{12} = \alpha\ \theta^q_{12}, \quad \theta_{13} = \alpha\ \theta^q_{13}, \quad \theta_{23} = \theta^q_{23}, \tag{17}$$

$$\textbf{Case 5}: \quad \theta_{12} = \theta^q_{12}, \quad \theta_{13} = \alpha\ \theta^q_{13}, \quad \theta_{23} = \alpha\ \theta^q_{23}, \tag{18}$$

$$\textbf{Case 6}: \quad \theta_{12} = \alpha\ \theta^q_{12}, \quad \theta_{13} = \theta^q_{13}, \quad \theta_{23} = \alpha\ \theta^q_{23}, \tag{19}$$

$$\textbf{Case 7}: \quad \theta_{12} = \alpha\ \theta^q_{12}, \quad \theta_{13} = \alpha\ \theta^q_{13}, \quad \theta_{23} = \alpha\ \theta^q_{23}. \tag{20}$$

The proportionality constant α in the above Eqs. (14-20) is taken as real parameter. We have carried out a detailed study for these cases in this work.

We note that there exist GUT models in the literature where proportionality between the quark and the leptonic mixing angles are explicitly shown. For example, the proportionality relation observed between the leptonic mixing angle θ_{13} and the Cabibbo angle θ_C in Eq. (2) can arise naturally in $SU(5)$ GUTs and Pati- Salam models. For more details, see [27]. Further more, it is shown in Ref. [18] that the relations between the quark and the leptonic mixing angles are possible and they support the idea of grand unification. However, non-abelian and abelian flavor symmetries are essential to make this happen [18] .

There is two-fold importance of the HSMR hypothesis. The first remarkable feature is that these relations provide a very simple way to achieve a large neutrino mixing. We shall see that predictions of these relations are easily testable in present and forthcoming

experiments. The second importance is that if predictions of HSMR hypothesis are confirmed by experimets, like neutrinoless double beta decay, this would be a strong hint of quark-lepton unification at high scale.

The plan of the paper is as follows. In section II, we present the required RG equations for the running of the neutrino mixing parameters. The SUSY threshold corrections and the neutrino mass scale are discussed in section III. The results are presented in section IV using dimensional-5 operator as well as in the framework of type-I seasaw. In section V, for the sake of illustration, we discuss two models where HSMR hypothesis can be realised. We summarize our results and conclude in section VI.

II. RG EVOLUTION OF THE LEPTONIC MIXING PARAMETERS

In this section, we briefly discuss the RG evolution of the leptonic mixing parameters.The most often studied scenario is the one where the Majorana mass term for the left handed neutrinos is given by the lowest dimensional operator [36]

$$\mathscr{L}_\kappa = \frac{1}{4}\kappa_{gf}\,\overline{\ell^{\rm C}_{\rm L}}{}^{g}_{c}\varepsilon^{cd}\phi_d\;\ell^{f}_{{\rm L}b}\varepsilon^{ba}\phi_a + \text{h.c.}\,, \tag{21}$$

in the SM. In the MSSM, it is given by

$$\mathscr{L}^{\rm MSSM}_\kappa \;=\; \mathscr{W}_\kappa\big|_{\theta\theta} + \text{h.c.} = -\tfrac{1}{4}\kappa_{gf}\,\mathbb{L}^{g}_{c}\varepsilon^{cd}\mathbb{h}^{(2)}_{d}\;\mathbb{L}^{f}_{b}\varepsilon^{ba}\mathbb{h}^{(2)}_{a}\big|_{\theta\theta} + \text{h.c.}\,, \tag{22}$$

where κ_{gf} has mass dimension -1, $\ell^{C}_{\rm L}$ is the charge conjugate of a lepton doublet and $a,b,c,d \in \{1,2\}$ are $\mathrm{SU}(2)_{\rm L}$ indices. The double-stroke letters $\mathbb{L}$ and $\mathbb{h}$ denote the lepton doublets and the up-type Higgs superfield in the MSSM. Using this mass operator, we introduce neutrino masses in a rather model independent way since it does not depend on the underlying mass mechanism.

The evolution of the above dimensional-5 operator below the scale where it is generated is provided by its RG equation. The one loop equation is as follows [37–40]

$$16\pi^2\,\dot\kappa \;=\; C\,(Y_e^\dagger Y_e)^T\,\kappa + C\,\kappa\,(Y_e^\dagger Y_e) + \hat\alpha\,\kappa\,, \tag{23}$$

where $\dot\kappa = \frac{d\kappa}{dt}$, $t = \ln(\mu/\mu_0)$ and μ is the renormalization scale and

$$C \;=\; 1 \qquad \text{in the MSSM}\,,$$

$$C \;=\; -\frac{3}{2} \quad \text{in the SM} \,. \tag{24}$$

The parameter $\hat{\alpha}$ in the SM and MSSM is given by

$$\begin{aligned} \hat{\alpha}_{\rm SM} \;&=\; -3g_2^2 + 2(y_\tau^2 + y_\mu^2 + y_e^2) + 6\left(y_t^2 + y_b^2 + y_c^2 + y_s^2 + y_d^2 + y_u^2\right) + \lambda \,, \\ \hat{\alpha}_{\rm MSSM} \;&=\; -\frac{6}{5}g_1^2 - 6g_2^2 + 6\left(y_t^2 + y_c^2 + y_u^2\right) \,. \end{aligned} \tag{25}$$

The quantities y_f ($f \in \{e, d, u\}$) represent the Yukawa coupling matrices of the charged leptons, down- and up-type quarks respectively, g_i ($i = 1, 2$) denote the gauge couplings and λ is the Higgs self coupling. For more details see Ref. [36].

We are interested in the RG evolution of parameters that are the masses, the mixing angles and the physical phases. The mixing angles and the physical phases are described by the PMNS matrix. This matrix is parameterized as follows

$$U_{PMNS} \;=\; V \cdot U, \tag{26}$$

where

$$V = \begin{pmatrix} c_{12}c_{13} & s_{12}c_{13} & s_{13}e^{-{\rm i}\delta} \\ -c_{23}s_{12} - s_{23}s_{13}c_{12}e^{{\rm i}\delta} & c_{23}c_{12} - s_{23}s_{13}s_{12}e^{{\rm i}\delta} & s_{23}c_{13} \\ s_{23}s_{12} - c_{23}s_{13}c_{12}e^{{\rm i}\delta} & -s_{23}c_{12} - c_{23}s_{13}s_{12}e^{{\rm i}\delta} & c_{23}c_{13} \end{pmatrix}, \tag{27}$$

and

$$U = \begin{pmatrix} e^{-{\rm i}\varphi_1/2} & 0 & 0 \\ 0 & e^{-{\rm i}\varphi_2/2} & 0 \\ 0 & 0 & 1 \end{pmatrix},$$

with c_{ij} and s_{ij} defined as $\cos\theta_{ij}$ and $\sin\theta_{ij}$ ($i, j = 1, 2, 3$), respectively. The quantity δ is the Dirac phase and φ_1, φ_2 are the Majorana phases. The global experimental status of the leptonic mixing parameter is summarized in Table I.

Here we would like to remark that the RG equations (23) for Yukawa couplings matrices are parametrization independent. The main aim is to probe if there is any connection between the quark and the leptonic mixing. For this purpose, we have chosen the standard parametrization which is the most studied and also commonly used in the literature. In principle, one could use an alternative parameterization to work and test the reality of HSMR. The results can be always interpreted as a possible indication of a connection between quark and leptonic mixing.

Quantity	Best Fit	3σ Range
Δm^2_{21} (10^{-5} eV^2)	7.54	6.99 – 8.18
Δm^2_{32} (10^{-3} eV^2)	2.39	2.20 – 2.57
θ°_{12}	33.71	30.59 – 36.81
θ°_{23}	41.38	37.7 – 52.3
θ°_{13}	8.8	7.63 – 9.89

TABLE I: The global fits for the neutrino mixing parameters [1].

We now summarize the RG equations used for running the leptonic mixing parameters from high to the low scale. For a detailed discussion of these equations, see Ref. [36]. These equations are derived using the lowest dimensional neutrino mass operator as discussed above and are given by the following analytical expressions [36]

$$\dot{\theta}_{12} \;=\; -\frac{Cy_\tau^2}{32\pi^2}\,\sin 2\theta_{12}\, s^2_{23}\,\frac{|m_1\, e^{\mathrm{i}\varphi_1} + m_2\, e^{\mathrm{i}\varphi_2}|^2}{\Delta m^2_{21}} + \mathscr{O}(\theta_{13})\;, \tag{28}$$

$$\begin{aligned}\dot{\theta}_{13} \;=\; & \frac{Cy_\tau^2}{32\pi^2}\,\sin 2\theta_{12}\,\sin 2\theta_{23}\,\frac{m_3}{\Delta m^2_{32}\,(1+\zeta)}\,\times \\ & \times\,[m_1\cos(\varphi_1-\delta) - (1+\zeta)\,m_2\,\cos(\varphi_2-\delta) - \zeta m_3\,\cos\delta] + \mathscr{O}(\theta_{13})\;,\end{aligned} \tag{29}$$

$$\begin{aligned}\dot{\theta}_{23} \;=\; & -\frac{Cy_\tau^2}{32\pi^2}\,\sin 2\theta_{23}\,\frac{1}{\Delta m^2_{32}}\left[c^2_{12}\,|m_2\, e^{\mathrm{i}\varphi_2} + m_3|^2 + s^2_{12}\,\frac{|m_1\, e^{\mathrm{i}\varphi_1} + m_3|^2}{1+\zeta}\right] \\ & + \mathscr{O}(\theta_{13})\;,\end{aligned} \tag{30}$$

where $\dot{\theta}_{ij} = \frac{d\theta_{ij}}{dt}$ (with $i, j = 1, 2, 3$), $t = \ln(\mu/\mu_0)$, μ being the renormalization scale and

$$\zeta \;:=\; \frac{\Delta m^2_{21}}{\Delta m^2_{32}}\;, \quad \Delta m^2_{21} := m_2^2 - m_1^2, \quad \Delta m^2_{32} := m_3^2 - m_2^2. \tag{31}$$

For the masses, the results for $y_e = y_\mu = 0$ but arbitrary θ_{13} are

$$16\pi^2\,\dot{m}_1 \;=\; \left[\hat{\alpha} + Cy_\tau^2\left(2s^2_{12}\,s^2_{23} + F_1\right)\right] m_1\;, \tag{32a}$$

$$16\pi^2\,\dot{m}_2 \;=\; \left[\hat{\alpha} + Cy_\tau^2\left(2c^2_{12}\,s^2_{23} + F_2\right)\right] m_2\;, \tag{32b}$$

$$16\pi^2\,\dot{m}_3 \;=\; \left[\hat{\alpha} + 2Cy_\tau^2\,c^2_{13}\,c^2_{23}\right] m_3\;, \tag{32c}$$

where $\dot{m}_i = \frac{dm_i}{dt}$ (i =1, 2, 3) and F_1, F_2 contain terms proportional to $\sin\theta_{13}$,

$$F_1 \;=\; -s_{13}\,\sin 2\theta_{12}\,\sin 2\theta_{23}\,\cos\delta + 2s^2_{13}\,c^2_{12}\,c^2_{23}\;, \tag{33a}$$

$$F_2 \;=\; s_{13}\,\sin 2\theta_{12}\,\sin 2\theta_{23}\,\cos\delta + 2 s_{13}^2\, s_{12}^2\, c_{23}^2\;. \tag{33b}$$

In this work, we are working in the CP conserving limit which means Majorana and Dirac phases are assumed to be zero. Therefore, we have not provided the RG equations for them. The non-zero phases are expected to have non-trivial impact on the parameter space. However, this study is beyond the scope of the present work and will be presented in a future investigation. Furthermore, we also study the effect of the new physics which could generate the above dimensional-5 operator. For this purpose, we present our analysis within the framework of type-I seesaw.

Now, we briefly discuss the evolution of the leptonic mixing angles. In the SM as can be seen from Eq. (25), only tau Yukawa coupling will dominate the evolution which is already very small. Hence the running of the neutrino masses is governed by a common scaling factor and the evolution of leptonic mixing angles can only be enhanced for QD mass pattern. In the MSSM the value of tau Yukawa coupling can be larger with respect to the value in the SM for a large value of $\tan\beta$. Hence the evolution of the leptonic mixing parameters can be enhanced in addition to the enhancement coming from the QD neutrino mass pattern as discussed below.

It is interesting to note from Eqs. (28, 29 and 30) that the major contribution to RG evolution of the mixing angles arises due to following enhancement factors

$$\dot{\theta}_{12} \propto \xi_1, \qquad \dot{\theta}_{13},\, \dot{\theta}_{23} \propto \xi_2, \tag{34}$$

where

$$\xi_1 \;=\; \frac{m^2}{\Delta m^2_{21}}, \qquad \xi_2 = \frac{m^2}{\Delta m^2_{32}}, \tag{35}$$

and m is the average neutrino mass with $m = (m_1 + m_2 + m_3)/3$. It is clear that we need masses of the neutrinos to be QD to explain the largeness of mixing angles at the low scale.

III. THE LOW ENERGY SUSY THRESHOLD CORRECTIONS AND THE ABSOLUTE NEUTRINO MASS SCALE

We discuss the required low energy SUSY threshold corrections for the mass square differences and the significance of the absolute neutrino mass scale in this section.

A. The low energy SUSY threshold corrections

It is well established in the previous works on HSMU hypothesis that among the five mixing parameters, one of the mass square differences (Δm^2_{21}) lies outside the 3σ global range [28–32]. As shown in the previous works, this mass square difference can be brought well within the 3σ global limit, if the low energy SUSY threshold corrections are incorporated to the mass square differences [28–32]. The importance of SUSY threshold corrections for QD neutrinos is discussed in Refs. [41–44]. These corrections are given by the following equations [29]

$$\begin{aligned}
(\Delta m^2_{21})_{th} &= 2\mathrm{m}^2 \cos 2\theta_{12}[-2\mathrm{T_e} + \mathrm{T}_\mu + \mathrm{T}_\tau], \\
(\Delta m^2_{32})_{th} &= 2\mathrm{m}^2 \sin^2\theta_{12}[-2\mathrm{T_e} + \mathrm{T}_\mu + \mathrm{T}_\tau], \\
(\Delta m^2_{31})_{th} &= 2\mathrm{m}^2 \cos^2\theta_{12}[-2\mathrm{T_e} + \mathrm{T}_\mu + \mathrm{T}_\tau].
\end{aligned} \tag{36}$$

where m is the mean mass of the QD neutrinos and the one loop factor $T_{\hat{\alpha}}(\hat{\alpha} = e, \mu, \tau)$ is given by [41, 44]

$$T_{\hat{\alpha}} = \frac{g_2^2}{32\pi^2}\left[\frac{x_\mu^2 - x_{\hat{\alpha}}^2}{y_\mu y_{\hat{\alpha}}} + \frac{(y_{\hat{\alpha}}^2 - 1)}{y_{\hat{\alpha}}^2} ln(x_{\hat{\alpha}}^2) - \frac{(y_\mu^2 - 1)}{y_\mu^2} ln(x_\mu^2)\right], \tag{37}$$

where g_2 is the $SU(2)$ coupling constant and $y_{\hat{\alpha}} = 1 - x_{\hat{\alpha}}^2$ with $x_{\hat{\alpha}} = M_{\hat{\alpha}}/M_{\tilde{w}}$; $M_{\tilde{w}}$ stands for wino mass, $M_{\hat{\alpha}}$ represents the mass of charged sleptons. We work with an inverted hierarchy in the charged-slepton sector where the mass of selectron is defined through the ratio $R = \frac{M_{\tilde{e}}}{M_{\tilde{\mu},\tilde{\tau}}}$. The mass of the wino is chosen to be 400 GeV following the direct searches at the LHC [45].

B. The absolute neutrino mass scale

The scale of the neutrino mass is one of the open questions, ever since it has been confirmed that the neutrinos are massive. In case of QD and the normal hierarchical spectra, we have

$$m_1 \lesssim m_2 \lesssim m_3 \simeq m_0 \tag{38}$$

with

$$m_0 \gg \sqrt{\Delta m^2_{32}} \approx 5 \times 10^{-2}\,\mathrm{eV}. \tag{39}$$

There are three complementary ways to measure the neutrino mass scale. The first one, a model independent method, is to use the kinematics of β-decay to determine the effective electron (anti) neutrino mass (m_β). It is given by

$$m_\beta \equiv \sqrt{\sum |U_{ei}|^2 \, m_i^2} \, . \tag{40}$$

The m_β has an upper bound of 2 eV from tritium beta decay [46, 47]. In future, the KATRIN experiment has sensitivity to probe m_β as low as 0.2 eV at 90% CL [48]. We note that m_0 in the QD regime for CP conservation is approximately equal to the effective beta decay mass m_β. Hence QD mass pattern is well within the sensitivity of the KATRIN.

The second method to extract the neutrino mass is neutrinoless double beta decay which assumes that neutrinos are Majorana particles [49, 50]. The observable parameter M_{ee}, the double beta decay effective mass is given as following

$$\begin{aligned} M_{ee} \; &= \; \left| \sum U_{ei}^2 \, m_i \right| , \\ &= \; \left| m_1 c_{12}^2 \, c_{13}^2 e^{-i\varphi_1} + m_2 s_{12}^2 \, c_{13}^2 \, e^{-i\varphi_2} + m_3 s_{13}^2 \, e^{-i2\delta} \right| . \end{aligned} \tag{41}$$

For quasi-degenerate neutrinos

$$M_{ee} \; \approx \; m_0 \left| c_{12}^2 \, c_{13}^2 e^{-i\varphi_1} + s_{12}^2 \, c_{13}^2 \, e^{-i\varphi_2} + s_{13}^2 \, e^{-i2\delta} \right| . \tag{42}$$

Since the contribution of m_3 is suppressed by the small $\sin^2\theta_{13}$ coefficient, we obtain

$$M_{ee} \simeq m_0 \sqrt{1 - \sin^2 2\theta_{12} \frac{(1 - \cos(\varphi_1 - \varphi_2))}{2}} . \tag{43}$$

For CP conserving case where the Majorana and Dirac phases are zero, $M_{ee} \simeq m_0$. For $M_{ee} \simeq 0.1$ eV, the above expression corresponds approximately to half-life in the range of 10^{25} to 10^{26} yrs [49] which makes the QD mass scheme testable in present and future experiments . In the QD regime, the neutrino mass can be written as [49]

$$m_0 \leq (M_{ee})^{\rm exp}_{\rm max} \, \frac{1 + \tan^2\theta_{12}}{1 - \tan^2\theta_{12} - 2\,|U_{e3}|^2} \equiv (M_{ee})^{\rm exp}_{\rm max} \, f(\theta_{12}, \theta_{13}) \, . \tag{44}$$

Using inputs from Table I, the function $f(\theta_{12}, \theta_{13})$ has a range from 2.2 to 4.1 at 3σ. The most stringent upper limit on the effective mass M_{ee} provided by the GERDA experiment is 0.4 eV [51]. Hence $m_0 \leq 1.64$ eV and sum of the neutrino masses $\Sigma m_i = 3m_0 \leq 4.91$ eV.

The third determination of neutrino masses is provided by the cosmological and astrophysical observations. The sum of the neutrino masses, Σm_i, has a range for upper bound to be $0.17 - 0.72$ eV at 95% CL [52]. This limit is not model independent and depends on the cosmological model applied to the data.

IV. RESULTS

We present our results in this section for the different cases listed in Eqs. (14 - 20) and for limiting cases of the most general HSMR as shown in Eqs. (5 - 11). As discussed earlier, we need MSSM as an extension of the SM for the implementation of HSMR and HSMU hypothesis. In the first step, we run quark mixing angles, gauge couplings, Yukawa couplings of quarks and charged leptons from the low scale to the SUSY breaking scale. The evolution from the SUSY breaking scale to the unification scale is done through the MSSM RG equations. After evolving up to the unification scale, we obtain quark mixing angles $\theta^q_{12} = 13.02^\circ$, $\theta^q_{13} = 0.17^\circ$ and $\theta^q_{23} = 2.03^\circ$. In the next step, quark mixing angles are used to calculate the leptonic mixing angles using HSMR at the unification scale. After this, we run down the MSSM RG equations up to the SUSY breaking scale. The SM RG equations take over the evolution of mixing parameters beyond the SUSY breaking scale. The SUSY breaking scale is chosen to be 2 TeV following the direct LHC searches [45]. We also need a large $\tan\beta$ which is chosen to be 55. The unification scale where HSMR can exist is chosen to be 10^{14} GeV which is consistent with present experimental observations [1]. We have used the MATHEMATICA based package REAP [53] for the numerical computation of our results. We have done a rigorous, thorough and comprehensive in this work. For this pupose, we have written an interface code which together with public code can be used to scan whole parameter space.

A. RG evolution of HSMR

We study the RG evolution of HSMR as given in Eqs. (14 - 20) and compare our results with respect to the HSMU hypothesis. In Fig. 1, we show how enhancement factors ξ_1 and ξ_2 evolve from the unification scale to the low scale, as α deviates from unity. The results are displayed for all the cases. It can be seen from Fig. 1 that the evolution in Case 1 at

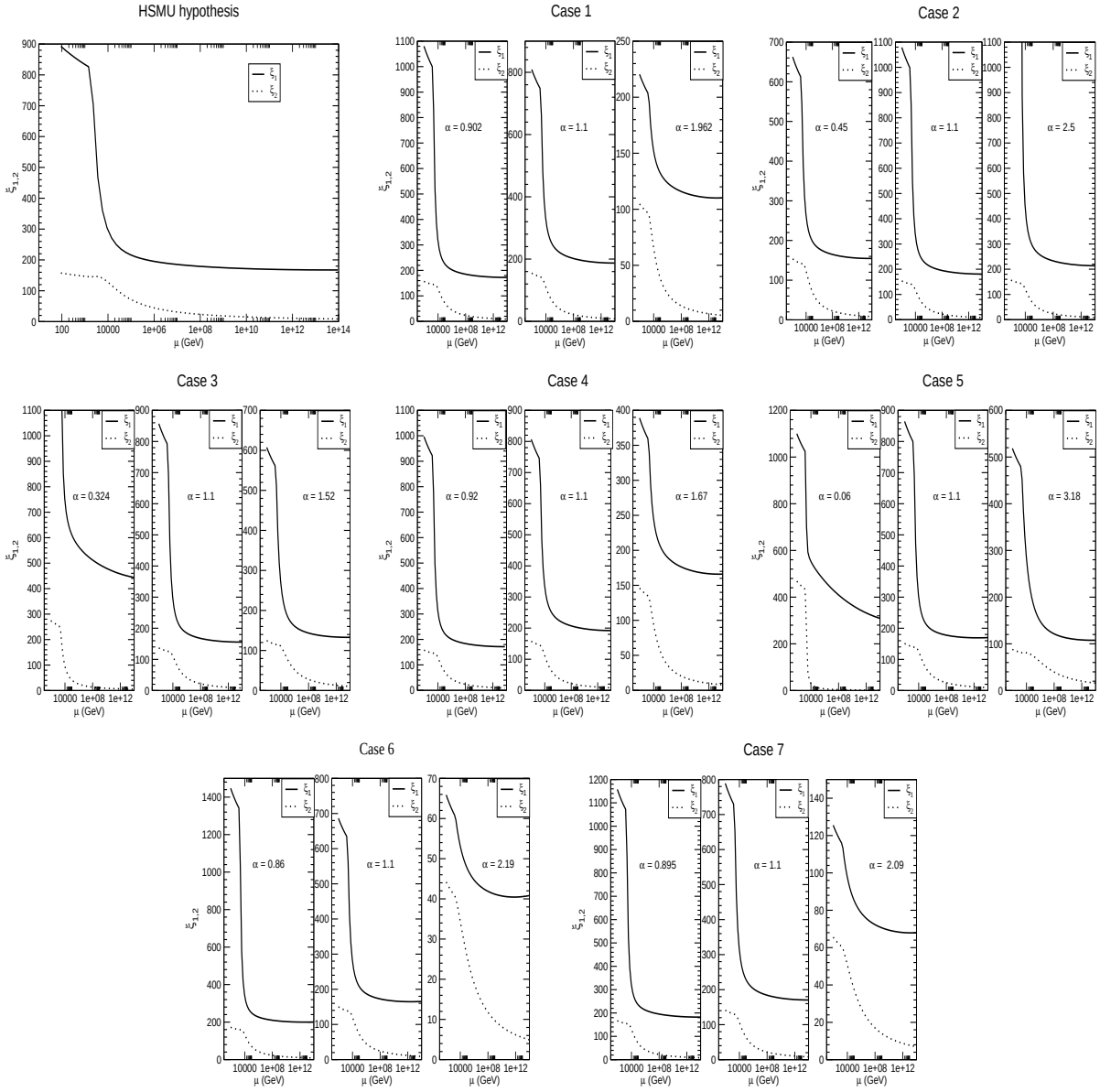

FIG. 1: The change in the RG evolution of the enhancement factors ($\xi_{1,2}$), 35, for the different cases of HSMR as a function of the RG scale μ when α deviates from unity.

$\alpha = 1.1$ is similar to HSMU hypothesis. However, as α approaches to lowest value on the left panel of Case 1, ξ_1 changes sufficiently. Similarly for the upper limit of $\alpha = 1.962$, the evolution again becomes very different from the HSMU hypothesis. This explains why the RG evolution of the PMNS mixing angles change when α deviates from unity. The same argument follows for all the other cases of HSMR and can be checked from Fig. 1.

We next show the evolution of the mixing angles for the different cases in Fig. 2 along

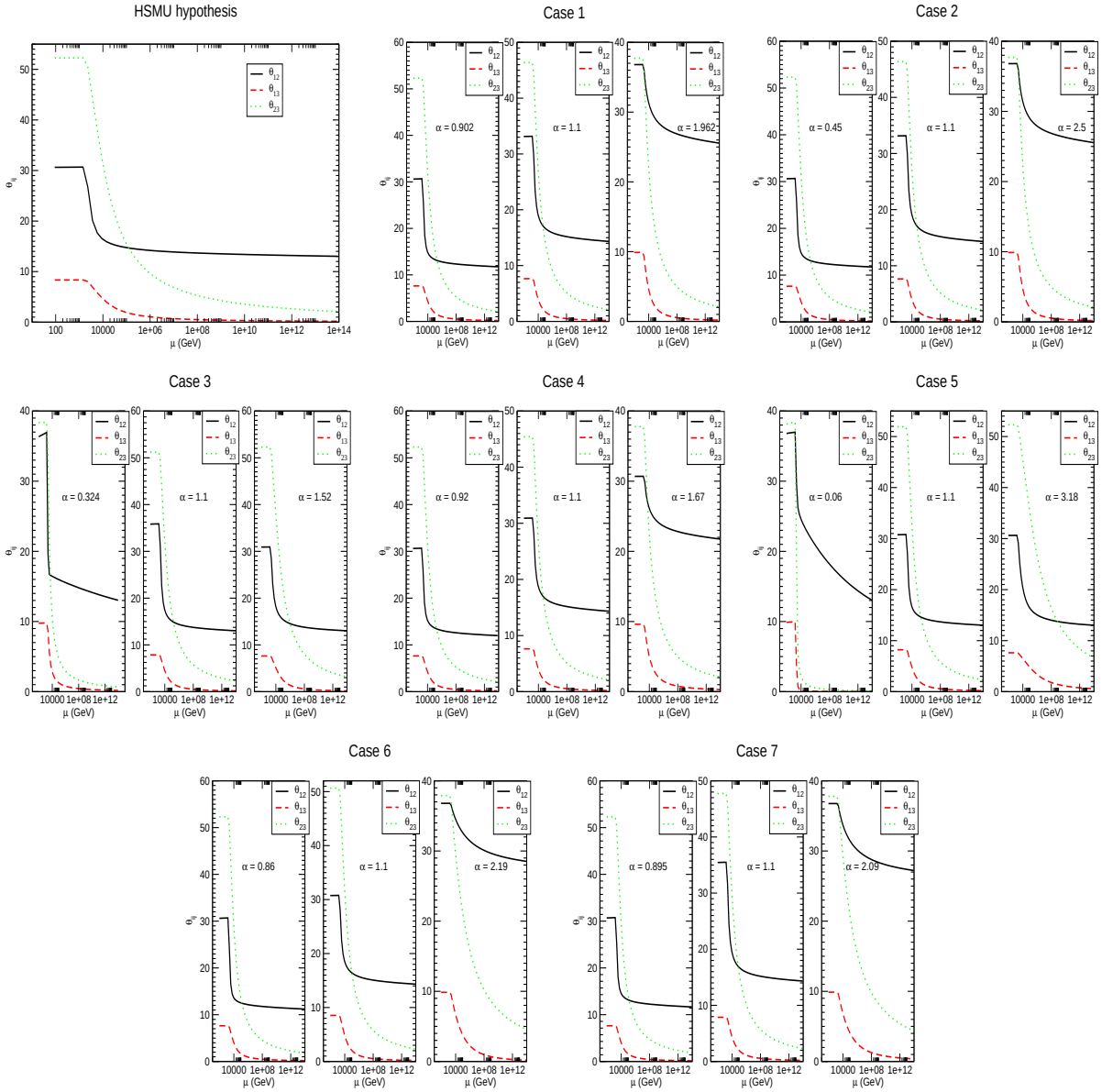

FIG. 2: The RG evolution of the PMNS mixing angles with respect to the RG scale μ, for the different cases, with α varied in the respective allowed range.

with the HSMU hypothesis. We observe from Figs. 1 and 2, that the evolution of HSMR is similar to the HSMU hypothesis when α deviates slightly from unity. However, when α is very far from unity, RG evolution undergoes dramatic changes. There is another interesting phenomenon that can be observed from Fig. 2. It can be easily seen that the RG evolution of the mixing angles, for Cases 3 and 5 are similar, with θ_{12} and θ_{23} almost similar at the low scale at the lower end of α. The difference between them at the low scale increases with

the increase in value of α. The pattern is exactly opposite in the other cases of HSMR, with the difference between θ_{12} and θ_{23} at the low scale decreasing as one goes from the lower to the upper end of α. This in a way tells us beforehand that the phenomenology of Case 3 and 5 will be similar, which will be discussed in detail afterwards.

B. Phenomenology of HSMR

In this subsection, we discuss in details the phenomenological implications of HSMR. Our aim is to investigate the behavior of α as it deviates from unity and its phenomenological consequences taking into account all the experimental constraints of Table I and the GERDA limit [51]. The common observation among all HSMR is the emergence of the strong correlations among Δm^2_{32}, M_{ee}, θ_{23}, θ_{13} and Σm_i.

1. HSMU hypothesis

As observed earlier, the value $\alpha = 1$ will reduce all cases of HSMR to HSMU hypothesis. We present a full parameter scan of the HSMU hypothesis using dimensional-5 operator. It should be noted that this analysis was absent in the previous works on HSMU hypothesis [32–34] and is reported in this work for the first time. We present a correlation in Fig. 3, which is not studied in the previous investigations. We show here the variation of Δm^2_{32} with respect to M_{ee}. The M_{ee} has an upper bound of 0.4 eV from the GERDA experiment [51]. Using this limit, we are able to put an upper bound on the allowed range of Δm^2_{32}. The allowed range for Δm^2_{32} is $(2.21 - 2.45) \times 10^{-3}$ eV^2 as observed from Fig. 3. The lower bound on M_{ee} is 0.384 eV for the HSMU hypothesis. Hence, our work on the HSMU hypothesis will be ruled out if GERDA crosses this number in the future. The effective β decay mass m_β is another interesting observable since it does not depend on whether the neutrinos are Majorana or Dirac. The prediction for m_β coincides with the effective double beta decay mass M_{ee} in the QD regime and for CP conservation. Hence, the allowed range for m_β is identical to that of M_{ee} in our work.

In Fig. 4, we show the variation of θ_{23} with respect to θ_{13}. We observe a strong correlation between θ_{13} and θ_{23}. The difference between this investigation and that of presented in Ref. [32] is the variation of θ_{12}. In the previous work, this correlation was reported for a

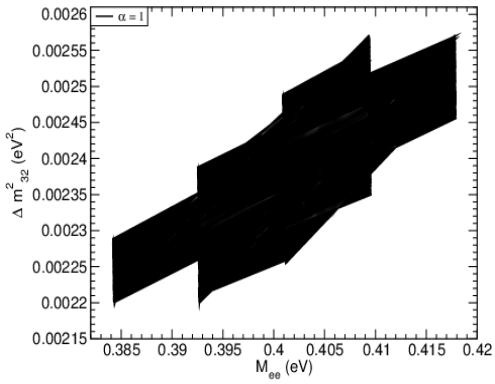

FIG. 3: The variation of Δm^2_{32} with respect to M_{ee}, in the context of the HSMU hypothesis, with α =1.

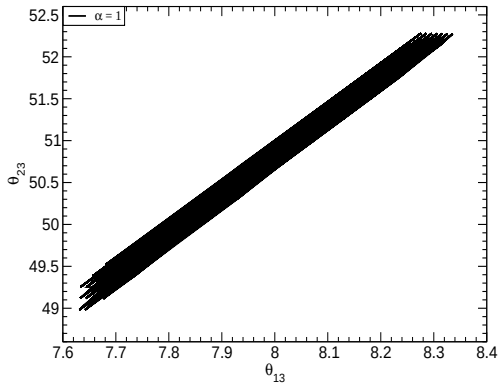

FIG. 4: The variation of θ_{23} with respect to θ_{13}, in the context of the HSMU hypothesis, with α =1.

chosen value of the angle θ_{12} at the low scale in the context of type I seesaw. In this work, we do not choose any particular value of θ_{12} at the low scale. We obtain a band for this correlation and previous results are a specific case of our present results. We observe that θ_{23} is non maximal and always lies in the second octant. This confirms the predictions of our earlier work [32]. The allowed range of θ_{13} is $7.63^\circ - 8.34^\circ$ and that of θ_{23} is $49^\circ - 52.3^\circ$.

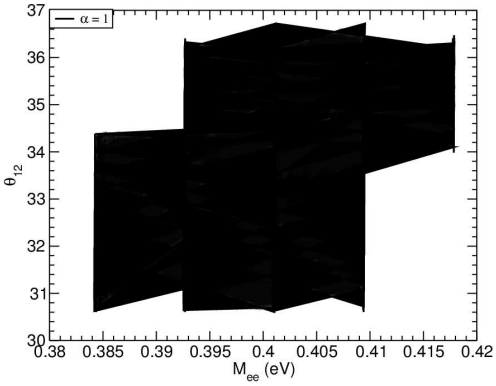

FIG. 5: The variation of θ_{12} with respect to M_{ee}, in the context of the HSMU hypothesis, with α =1.

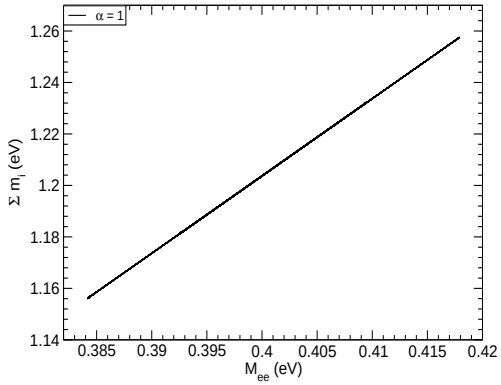

FIG. 6: The variation of Σm_i with respect to M_{ee}, in the context of the HSMU hypothesis, with α =1.

We next present variation of θ_{12} against M_{ee} in Fig. 5. This correlation is also a new prediction of our work and do not exist in previous studies. The whole 3σ global range for

the angle θ_{12} is allowed for the $M_{ee} \leq 0.4$ eV, However, as can be observed from Fig. 5, the range $34.4^\circ \leq \theta_{12} \leq 36.81^\circ$ is ruled out for 0.384 eV $\leq M_{ee} \leq$ 0.393 eV. The precise predictions for all observables are provided in Table III. In the end, we also have a new correlation between the sum of neutrino masses and M_{ee} which is not studied previously. This correlation is shown in Fig. 6. Our prediction for sum of neutrino masses is $1.16 - 1.2$ eV using the upper bound on M_{ee} given by the GERDA.

2. The most general HSMR within the same generations

The most general HSMR within the same generations for $(k_1, k_2, k_3) = (1, 1, 1)$ as defined before is given by the following equation

$$\theta_{12} = \alpha_1\ \theta^q_{12}, \quad \theta_{13} = \alpha_2\ \theta^q_{13}, \quad \theta_{23} = \alpha_3\ \ \theta^q_{23}. \tag{45}$$

We present the results for the maximum and the minimum values of α_i for Eqs. (5-12), taking into account all the experimental constriants. In the Table II, we present the allowed values of α_i along with the the respective physical masses and the mixing angles.

It is remarkable that in the Case E, all the mixing parameters are within 3σ global range without adding threshold corrections. If we add threshold corrections, the predictions are $\Delta m^2_{32} = 2.35 \times (10^{-3}\text{eV}^2)$ and $\Delta m^2_{21} = 7.01 \times (10^{-5}\text{eV}^2)$ for $R = 1.0$. Thus, threshold corrections at this point are effectively negligible. We further notice that the different combinations of the allowed end points of α_i, leads to M_{ee} around 0.35 eV - 0.4 eV. This most general case with different α_i, alone will not suffice, when the value of M_{ee} will be further constrained by the future experiments. We then have to look for more specific cases, where the α_i's will not be different, but have some relations among them. We consider the simplified scenario, where the α_i's are equal. We have carried out a detailed analysis for all the possible seven cases in this scenario in the next subsections.

3. Case 1: $\theta_{12} = \alpha\ \theta^q_{12}, \quad \theta_{13} = \theta^q_{13}, \quad \theta_{23} = \theta^q_{23}$

The first case of HSMR is the one where leptonic mixing angle θ_{12} is proportional to θ^q_{12} and the other two angles are identical. In Fig. 7, we show how the correlation between Δm^2_{32} and M_{ee} changes as α deviates from unity. We observe on the left panel of Fig. 7

	α_1	α_2	α_3	Masses at unification scale (eV)			Σm_i (eV)	θ_{12}°	θ_{13}°	θ_{23}°	Δm^2_{32} (10^{-3}eV^2)	Δm^2_{21} (10^{-5}eV^2)	M_{ee} (eV)	Lightest neutrino mass: m_1 (eV)	R
				m_1	m_2	m_3									
Case A	1.46	2.54	1.19	0.4583	0.461	0.5186	1.16	36.52	9.88	41.14	2.5	8.06	0.385	0.3850	2.29
Case B	1.45	1.68	0.91	0.4757	0.478	0.5380	1.20	30.61	8.79	37.97	2.25	8.12	0.40	0.3997	1.8
Case C	1.38	0.71	1.28	0.489	0.493	0.5527	1.24	36.8	9.87	50.83	2.22	8.14	0.411	0.4106	5.3
Case D	1.14	0.92	0.94	0.4754	0.478	0.5370	1.20	31.18	7.70	45.31	2.20	8.14	0.40	0.3994	1.69
Case E	0.8	2.2	1.15	0.4096	0.412	0.4625	1.04	32.77	7.65	48.13	2.35	7.01	0.344	0.3442	-
Case F	0.89	1.61	0.82	0.4751	0.477	0.5361	1.20	30.6	7.65	43.66	2.22	7.37	0.40	0.3993	1.06
Case G	0.92	0.98	1.03	0.4421	0.445	0.4989	1.12	32.37	7.64	52.19	2.22	7.86	0.372	0.3714	1.48
Case H	0.88	0.95	0.86	0.4764	0.479	0.5372	1.20	30.99	7.63	51.97	2.22	7.55	0.40	0.4003	1.29

TABLE II: The allowed predictions for the different cases of the most general HSMR for minimum and maximum allowed values of α_i, Eqs. (5-11).

that the lowest allowed value of α is 0.902. This value is derived by the 3σ global limit of the leptonic mixing angles. On the right panel of Fig. 7, the upper bound on α is shown. For the upper bound on α, in principle, one can go up to 1.962 with all mixing parameters within the global range. This value of α belongs to $M_{ee} > 0.4$ eV and hence is ruled out by the GERDA limit. The allowed upper bound on α is 1.28 which is derived using the GERDA limit.

We compare Fig. 7 with Fig. 3 of the HSMU hypothesis ($\alpha = 1$) to study the phenomenological behavior of α. As obvious from the left panel of Fig. 7 , M_{ee} has its maximum allowed range at the lowest value of α. This is because the absolute neutrino mass decreases for $\alpha < 1$ and increases for $\alpha > 1$ in the case under study. Hence, at $\alpha = 0.902$ on the left panel of Fig. 7, we obtain 0.365 eV $\leq M_{ee} \leq$ 0.40 eV corresponding to whole 3σ global range of Δm^2_{32}. The same prediction for the HSMU hypothesis in Fig. 3, ($\alpha = 1$)

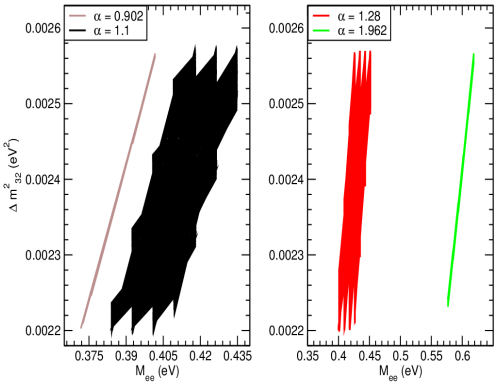

FIG. 7: The variation of Δm^2_{32} with respect to M_{ee} for Case 1 of HSMR.

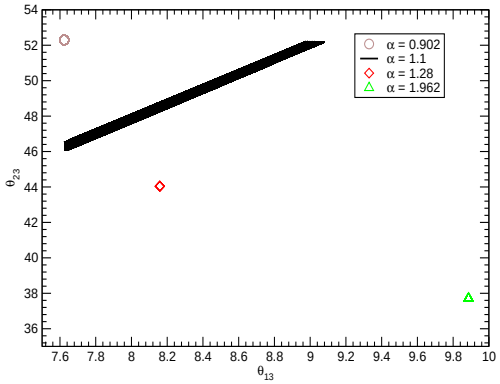

FIG. 8: The variation of θ_{23} with respect to θ_{13} for Case 1 of HSMR.

is 0.385 eV $\leq M_{ee} \leq$ 0.418 eV which belongs to $\Delta m^2_{32} = (2.21 - 2.45) \times 10^{-3}$ eV^2. The prediction when α slightly deviates from unity ($\alpha = 1.1$) is 0.384 eV $\leq M_{ee} \leq$ 0.435 eV corresponding to $\Delta m^2_{32} = (2.22 - 2.57) \times 10^{-3}$ eV^2. At the upper allowed value of $\alpha = 1.28$, we have 0.4 eV $\leq M_{ee} \leq$ 0.45 eV which belongs to $\Delta m^2_{32} = (2.20 - 2.57) \times 10^{-3}$ eV^2. We observe that the uppermost value of $\alpha = 1.962$ has 0.571 eV $\leq M_{ee} \leq$ 0.625 eV belonging to $\Delta m^2_{32} = (2.23 - 2.57) \times 10^{-3}$ eV^2. This value of α is already ruled out by the GERDA limit.

This case can be ruled out if GERDA reaches $M_{ee} <$ 0.365 eV. There is an apparent overlap between predictions of the case under study and the HSMU hypothesis. This can be discriminated using the SUSY ratio R. For a clear picture of the phenomenological consequences, we provide values of mixing parameters and other observables belonging to minimum and maximum allowed values of α for each case and the HSMU hypothesis in Table III.

The variation of θ_{23} with respect to θ_{13} is shown in Fig. 8. The mixing angles reach their 3σ limits at their lower and upper ends. For example, at $\alpha = 0.902$, θ_{13} is at its minimum of the 3σ global limit while θ_{23} is at its maximum independent of the upper bound of M_{ee}. On the other hand, at $\alpha = 1.962$, the predictions are reversed but this value is already rejected by the GERDA limit of M_{ee}. The allowed ranges of θ_{13} and θ_{23}, at $\alpha = 1.1$, are $7.62^\circ - 9.1^\circ$ and $46.09^\circ - 52.2^\circ$ respectively. Compared to Fig. 4 for the HSMU hypothesis where the allowed range of θ_{23} is always in the second octant, θ_{23} has its minimum value 44.04° at

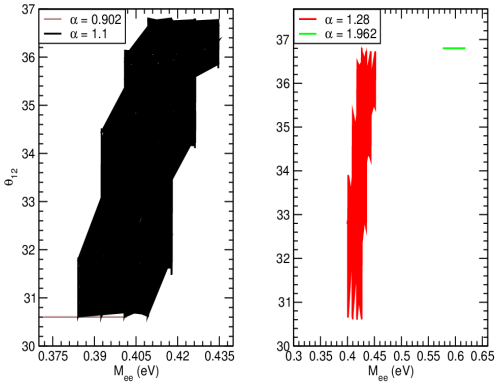

FIG. 9: The variation of θ_{12} with respect to M_{ee} for Case 1 of HSMR.

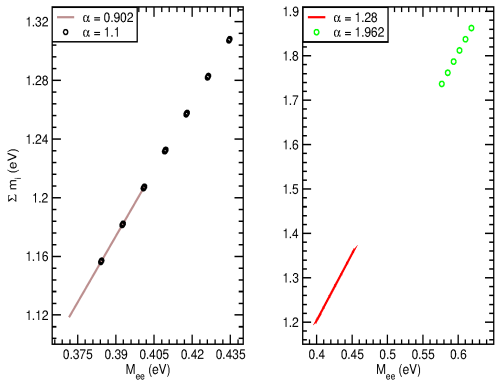

FIG. 10: The variation of Σm_i with respect to M_{ee} for Case 1 of HSMR.

$\alpha = 1.28$ which belongs to $M_{ee} = 0.4$ eV and lies in the first octant. The corresponding value of θ_{13} is 8.16°.

We next show the behavior of θ_{12} with respect to M_{ee} in Fig. 9. We observe that at $\alpha = 0.902$, θ_{12} is at its global minimum 30.6°. On the left panel of Fig. 9, at $\alpha = 1.1$, θ_{12} has an allowed range of $30.6° - 35.65°$ for $M_{ee} \leq 0.4$ eV. For the HSMU hypothesis in Fig. 5, θ_{12} has the whole 3σ global range with some higher values ruled out for $M_{ee} \leq 0.393$ eV. For $\alpha = 1.28$, the value of θ_{12} is 32.82° for $M_{ee} = 0.4$ eV as can be seen from the right panel of the figure. For $\alpha = 1.962$, θ_{12} reaches to the maximum of its 3σ global limit.

Finally in Fig. 10, the variation of sum of the neutrino masses with respect to M_{ee} is presented. For lowest value of $\alpha = 0.902$, on the left panel, the range of Σm_i is $1.12 - 1.2$ eV for $M_{ee} \leq 0.4$ eV. At $\alpha = 1.1$, it is $1.16 - 1.2$ eV for $M_{ee} \leq 0.4$ eV. On the right panel, the value of sum at $\alpha = 1.28$ is 1.2 eV and the region $\Sigma m_i > 1.2$ eV belongs to $M_{ee} > 0.4$ eV.

4. *Case 2:* $\theta_{12} = \theta_{12}^q, \quad \theta_{13} = \alpha\, \theta_{13}^q, \quad \theta_{23} = \theta_{23}^q$

The second case which we consider has leptonic mixing angle θ_{13} proportional to θ_{13}^q. In this case, the lower bound on α is 0.45 which is derived using global limits on the mixing angles. The α on the upper side, however, is remarkably bounded by the ratio R. This theoretical bound arises because we work with an inverted hierarchy in the charged-slepton sector and at $\alpha = 2.5$, we have $R = 1$. In principle, α has a range up to 3.5 satisfying all experimental constraints with $R < 1$.

In Fig. 11, we show the behavior of Δm^2_{32} versus M_{ee} for different values of α. For the $\alpha = 0.45$ on the right panel, we have 0.382 eV $\leq M_{ee} \leq$ 0.418 eV which corresponds to the whole 3σ global range of Δm^2_{32}. In case of $\alpha = 1.1$ on the left panel, 0.38 eV $\leq M_{ee} \leq$ 0.428 eV belongs to $\Delta m^2_{32} = (2.2 - 2.57) \times 10^{-3}$ eV^2. The range of M_{ee} at the upper end $\alpha = 2.5$ is 0.342 eV $\leq M_{ee} \leq$ 0.378 eV corresponding to $\Delta m^2_{32} = (2.2 - 2.53) \times 10^{-3}$ eV^2. A remarkable feature emerges in this case. Unlike case 1, the absolute neutrino mass scale increases for $\alpha < 1$ and decreases for $\alpha > 1$. Now, at the upper allowed value of $\alpha = 2.5$, M_{ee} is sufficiently below the GERDA limit. We would emphasize that one of the main observations of this case is that α is not constrained by the GERDA limit on either side. These results can easily be tested by GERDA in the near future.

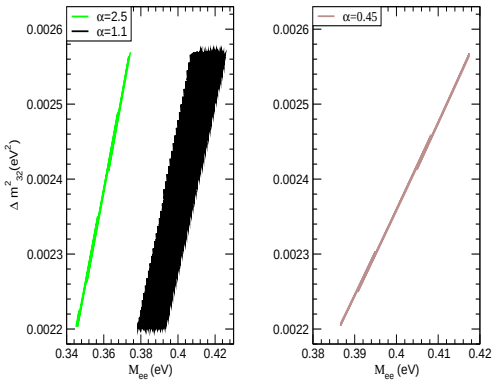

FIG. 11: The variation of Δm^2_{32} with respect to M_{ee} for Case 2 of HSMR.

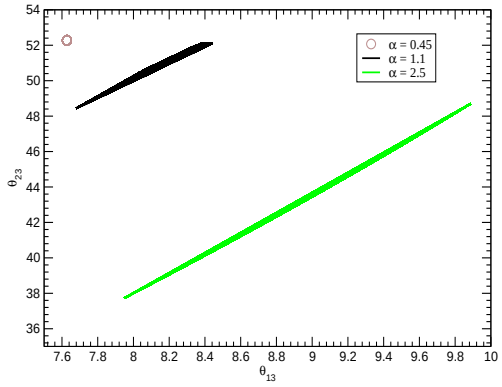

FIG. 12: The variation of θ_{23} with respect to θ_{13} for Case 2 of HSMR.

We show the variation of θ_{23} with respect to θ_{13} in Fig. 12. As can be seen, for the lowest possible value of $\alpha = 0.45$, the allowed range is just a point which is located at $\theta_{13} = 7.65°$ and $\theta_{23} = 52.5°$. As $\alpha = 1.1$, the range of θ_{13} is $7.65° - 8.4°$ and that of θ_{23} is $48.5° - 52.5°$. Finally for the highest value of $\alpha = 2.5$, θ_{13} has almost the whole 3σ range $7.92° - 9.88°$ and the range of θ_{23} is $36.8° - 48°$. These results can be contrasted to case 1 where the minimum of the mixing angle $\theta_{23} = 44.04°$ also happens for the upper value of α namely $\alpha = 1.28$ and in both cases, the value of θ_{23} can be in the first octant, contrary to the HSMU hypothesis. Also in both cases, the maximum of the mixing angle of θ_{23} corresponds to the lower value of alpha.

The next to be considered is the variation of θ_{12} versus M_{ee} as is shown in Fig. 13. In

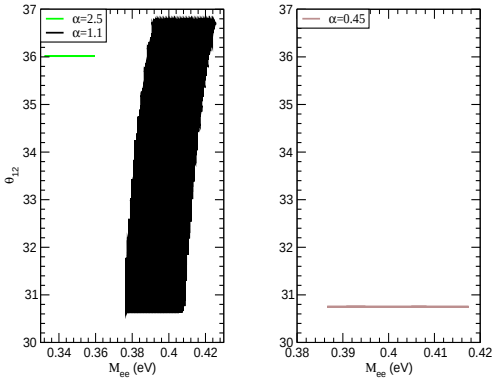

FIG. 13: The variation of θ_{12} with respect to M_{ee} for Case 2 of HSMR.

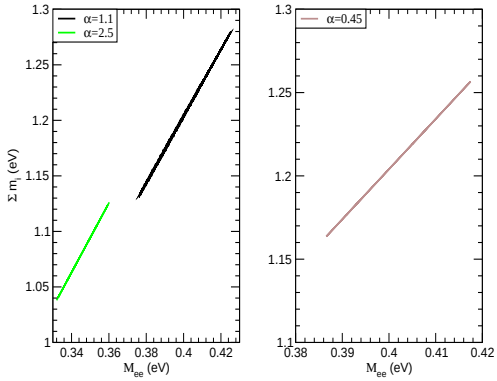

FIG. 14: The variation of Σm_i with respect to M_{ee} for Case 2 of HSMR.

the right panel it can be observed that $\alpha = 0.45$ corresponds to the minimum $\theta_{12} = 30.8°$ and 0.384 eV $\leq M_{ee} \leq$ 0.42 eV. For $\alpha = 1.1$ on the left panel, the whole 3σ range for θ_{12} is allowed for 0.39 eV $\leq M_{ee} \leq$ 0.4 eV and for $M_{ee} \leq$ 0.39 eV the allowed range of θ_{12} decreases. The upper value of $\alpha = 2.5$, on the left panel, corresponds $\theta_{12} = 36.02°$ while 0.344 eV $\leq M_{ee} \leq$ 0.366 eV.

In Fig. 14, we show the behavior of the sum of the neutrino masses with respect to M_{ee}. As can be seen in the right panel, for the lowest value of $\alpha = 0.45$, Σm_i lies in the range $1.16 - 1.2$ eV which corresponds to 0.383 eV $\leq M_{ee} \leq$ 0.4 eV. For $M_{ee} >$ 0.4, the range of Σm_i is $1.2 - 1.26$ eV. For the upper value of $\alpha = 2.5$, we have $\Sigma m_i = 1.05 - 1.12$ eV while 0.342 eV $\leq M_{ee} \leq$ 0.366 eV. On the left panel, for $\alpha = 1.1$, the range of Σm_i is $1.13 - 1.2$ eV which corresponds to 0.36 eV $\leq M_{ee} \leq$ 0.4 eV and the rest of the data point corresponds to $M_{ee} >$ 0.4 eV.

5. *Case 3:* $\theta_{12} = \theta^q_{12}, \quad \theta_{13} = \theta^q_{13}, \quad \theta_{23} = \alpha\ \theta^q_{23}$

We now consider the final case where two of the leptonic mixing angles θ_{12}, θ_{13} are identical to the quark mixing angle θ^q_{12}, θ^q_{13} and the third leptonic mixing angle θ_{23} is proportional to the quark mixing angle θ^q_{23}. The correlation between Δm^2_{32} and M_{ee} is shown in Fig. 15. The minimum allowed value of α, with all the mixing parameters within the global range, is 0.324. However in this case as can be seen from the right panel of Fig. 15, we have 0.62 eV $\leq M_{ee} \leq$ 0.66 eV. This value of α corresponds to the entire

3σ range of Δm^2_{32} and violates the upper limit from GERDA. Therefore we also consider the lower value of $\alpha = 0.89$, with all the mixing parameters within the global range and 0.4 eV $\leq M_{ee} \leq$ 0.43 eV. This value corresponds to the entire 3σ range of Δm^2_{32}. The prediction of M_{ee} at $\alpha = 1.1$ is 0.372 eV $\leq M_{ee} \leq$ 0.41 eV corresponding to the entire 3σ range of Δm^2_{32}. The upper allowed value of α in this case is 1.52, (left panel of Fig. 15) with 0.3 eV $\leq M_{ee} \leq$ 0.34 eV and having the entire 3σ range of Δm^2_{32}. Hence, the allowed range of α in this case covers the entire 3σ range of Δm^2_{32}. The absolute neutrino mass scale increases for $\alpha < 1$ and decreases for $\alpha > 1$ similar to Case 2. The behavior of α in this case, Fig. 15 is different from Case 1, Fig. 7, with the lower end of α constraining M_{ee}. In this case it is possible to reach values of M_{ee} as low as 0.3 eV compared to Cases 1, 2 and the HSMU hypothesis, and will only be ruled out if the limit from GERDA reaches $M_{ee} <$ 0.3 eV.

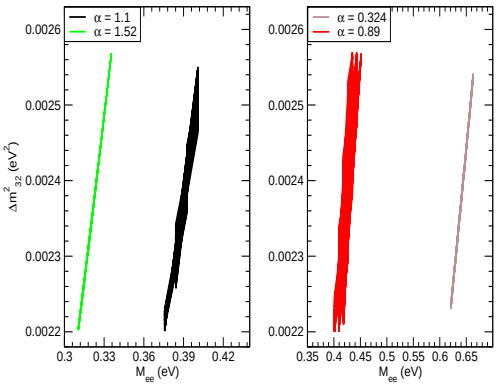

FIG. 15: The variation of Δm^2_{32} with respect to M_{ee} for Case 3 of HSMR.

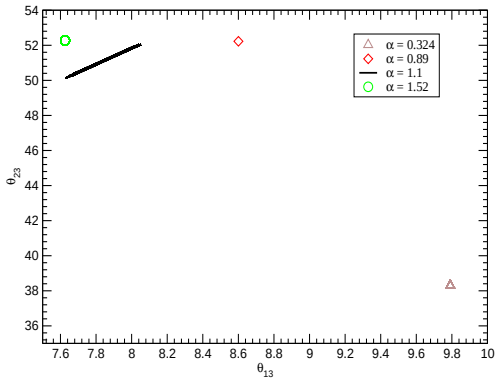

FIG. 16: The variation of θ_{23} with respect to θ_{13} for Case 3 of HSMR.

We next show the correlation of θ_{23} with respect of θ_{13} in Fig. 16. The θ_{23} and θ_{13} reach their 3σ global limits at the lowest and upper most end of α. The value of θ_{13} is 8.56° and that of θ_{23} is 52.4° for lower allowed value of $\alpha = 0.89$, corresponding to $M_{ee} = 0.4$ eV. The allowed ranges of θ_{13} and θ_{23} for $\alpha = 1.1$ in this case are much more constrained compared to Cases 1, 2 and the HSMU hypothesis. They are $7.62° - 8.05°$ and $50.1° - 52.1°$ respectively. The upper end of $\alpha = 1.52$, results in a minimum value of θ_{13}, whereas θ_{23} is at maximum with $\theta_{23} = 52.4°$. The behavior of α here is different from Cases 1 and 2 with the lower end of α resulting in the upper end point of θ_{13} and lower end point of θ_{23}.

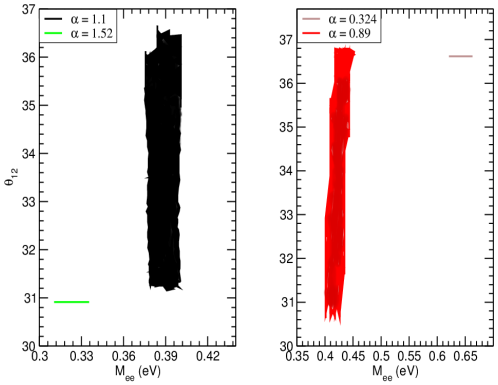

FIG. 17: The variation of θ_{12} with respect to M_{ee} for Case 3 of HSMR.

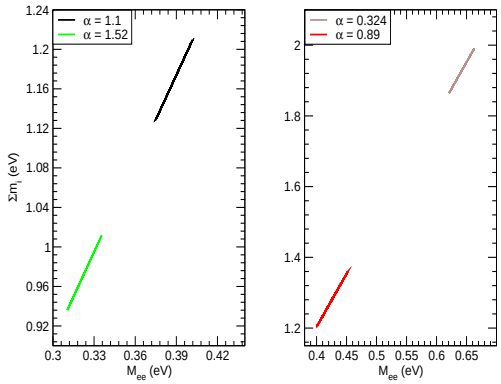

FIG. 18: The variation of Σm_i with respect to M_{ee} for Case 3 of HSMR.

In Fig. 17, we show the variation of θ_{12} with M_{ee}. We observe that the lower (30.78°) and upper (36.7°) 3σ global limits of θ_{12}, are reached at the upper most and the lowest ends of α respectively. In case of $\alpha = 0.89$, the value of θ_{12} is 30.62° which belongs to $M_{ee} = 0.4$. The whole 3σ global range of θ_{12} is allowed for $\alpha = 1.1$.

Finally we show in Fig. 18, the variation of the sum of the neutrino masses with respect to M_{ee}. The region with $M_{ee} \geq 0.4$ eV for $\alpha = 0.324$, has Σm_i in the range of $1.84 - 2$ eV and for $\alpha = 0.89$ it is in the range $1.2 - 1.38$ eV. In case of $\alpha = 1.1$, with $M_{ee} < 0.4$ eV, Σm_i is in the range $1.12 - 1.2$ eV. The upper end of $\alpha = 1.52$ has the sum in the range of $0.93 - 1.01$ eV. It is seen that Σm_i and M_{ee} is much more relaxed compared to the HSMU and Cases 1, 2.

6. *Case 4:* $\theta_{12} = \alpha\ \theta^q_{12}, \quad \theta_{13} = \alpha\ \theta^q_{13}, \quad \theta_{23} = \theta^q_{23}$

We now consider the case where the leptonic mixing angles θ_{12}, θ_{13} are proportional to the corresponding quark mixing angles $\theta^q_{12}, \theta^q_{13}$ and the leptonic mixing angle θ_{23} is identical to the quark mixing angle θ^q_{23}. The lowest allowed value of α for Case 4 is 0.92 which is derived using the 3σ global limits on mixing angles. The upper allowed value of α, respecting the GERDA limit, is 1.67. When we relax the GERDA limit then α turns out to be 1.77 satisfying the 3σ global limits. We show, the correlation between Δm^2_{32} and M_{ee} in Fig. 19. The lowest value of $\alpha = 0.92$, covers the range 0.38 eV $\leq M_{ee} \leq 0.4$ eV which corresponds to $\Delta m^2_{32} = (2.30 - 2.50) \times 10^{-3}$ eV^2 (cf. left panel of Fig. 19). The prediction of M_{ee} for

$\alpha = 1.1$ is 0.384 eV $\leq M_{ee} \leq$ 0.41 eV corresponding to the whole 3σ global range of Δm^2_{32}. On the right panel, the upper allowed end of $\alpha = 1.67$ has 0.4 eV $\leq M_{ee} \leq$ 0.42 eV with $\Delta m^2_{32} = (2.30 - 2.49) \times 10^{-3}$ eV^2. The upper most end $\alpha = 1.77$ where the GERDA limit is not satisfied, has 0.46 eV $\leq M_{ee} \leq$ 0.48 eV corresponding to $\Delta m^2_{32} = (2.37 - 2.53) \times 10^{-3}$ eV^2, as shown in the right panel of Fig. 19. The behavior of α is similar to Case 1 with the upper values of α being constrained by the GERDA limit. The first distinction that this case offers, with the others considered before is that the whole 3σ range of Δm^2_{32} is not covered in Case 4 for all the allowed values of α.

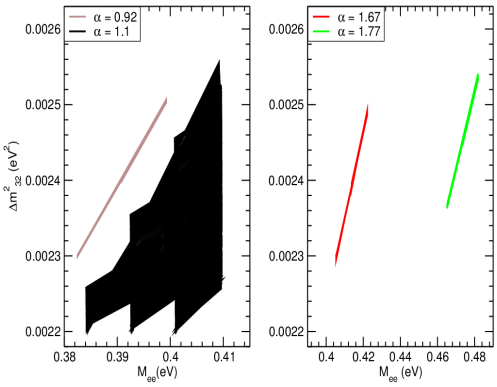

FIG. 19: The variation of Δm^2_{32} with respect to M_{ee} for Case 4 of HSMR.

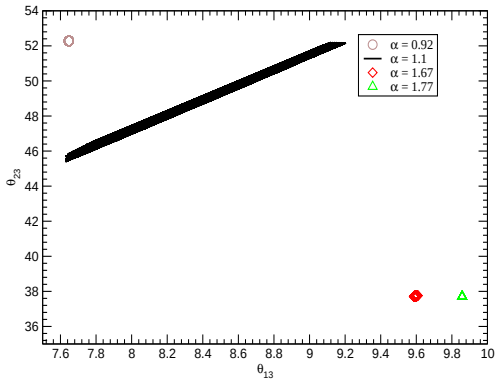

FIG. 20: The variation of θ_{23} with respect to θ_{13} for Case 4 of HSMR.

Next, we show the correlation between θ_{23} and θ_{13} as illustrated in Fig. 20. The lower end of $\alpha = 0.92$ reaches to the minimum of its 3σ global limit for θ_{13} and the maximum of the 3σ limit for θ_{23}. The situation for the upper most end of $\alpha = 1.77$, is just opposite to the lower end, i.e. θ_{13} is at the maximum of the 3σ global limit whereas θ_{23} is at its global minimum. This observation is just opposite to Case 3, where θ_{13} (θ_{23}) reaches the global minimum (maximum), at the upper end of α. The allowed ranges of θ_{13} and θ_{23}, at $\alpha = 1.1$ for this case are $7.62^\circ - 9.2^\circ$ and $45.41^\circ - 52.17^\circ$, respectively. The value of θ_{13} is 9.59° and that of θ_{23} is $37.71^\circ - 37.76^\circ$, for $\alpha = 1.67$.

The variation of θ_{12} with respect to M_{ee} is shown in Fig. 21. The lower and upper 3σ global limits of θ_{12} are obtained at the lower and upper most end of α respectively. This observation is in contrast with Case 3 and Case 5 (to be discussed later). We get the full range of θ_{12} (cf. Fig. 21 for details) for $\alpha = 1.1$, with some higher values of θ_{12} being ruled

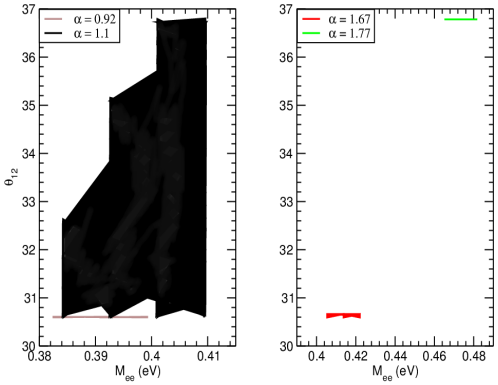

FIG. 21: The variation of θ_{12} with respect to M_{ee} for Case 4 of HSMR.

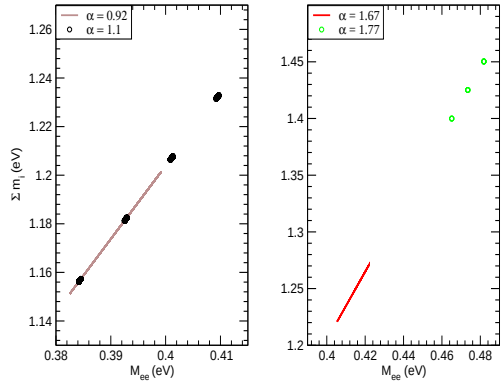

FIG. 22: The variation of Σm_i with respect to M_{ee} for Case 4 of HSMR.

out for $M_{ee} \leq 0.394$ eV. The value of θ_{12} at $\alpha = 1.67$ is $30.59° - 30.66°$.

Finally, we show the variation of the sum of neutrino masses with respect to M_{ee} in Fig. 22. We find that for the lowest value of $\alpha = 0.92$, the sum of neutrino mass ranges between $1.15 - 1.20$ eV for 0.38 eV $\leq M_{ee} \leq$ 0.4 eV. In case of $\alpha = 1.1$, Σm_i has a range of $1.157 - 1.23$ eV corresponding to 0.38 eV $\leq M_{ee} \leq$ 0.41 eV as can be seen from the left panel of Fig. 22. A close look at the right panel of Fig. 22 reveals that for $\alpha = 1.67$, Σm_i is in the range $1.22 - 1.27$ eV corresponding to 0.4 eV $\leq M_{ee} \leq$ 0.42 eV. The range for Σm_i turns out to be $1.4 - 1.45$ eV for $\alpha = 1.77$ which corresponds to $M_{ee} >$ 0.4 eV.

7. *Case 5:* $\theta_{12} = \theta_{12}^q, \quad \theta_{13} = \alpha\ \theta_{13}^q, \quad \theta_{23} = \alpha\ \theta_{23}^q$

We now look at the case of the leptonic mixing angle θ_{12} being identical with its CKM counterpart and the other two leptonic mixing angles being proportional to the quark mixing angles. The correlation between Δm^2_{32} and M_{ee} is shown in Fig. 23 as α deviates from unity. The minimum allowed value of α, with all the mixing parameters within the global range, is 0.06. However in this case as can be seen from the right panel of Fig. 23, we have 2.24 eV $\leq M_{ee} \leq$ 2.28 eV, which violates the upper limit from GERDA. Therefore including the constraints of GERDA, the lowest possible value of α becomes 0.89. For $\alpha = 0.89$, as can be seen from the right panel of Fig. 23, we obtain 0.40 eV $\leq M_{ee} \leq$ 0.42 eV corresponding to $\Delta m^2_{32} = (2.20 - 2.48) \times 10^{-3}$ eV^2. The prediction of M_{ee} for α=1.1 from the left panel of Fig. 23 is 0.36 eV $\leq M_{ee} \leq$ 0.41 eV which belongs to the whole 3σ range of Δm^2_{32}. The upper

allowed value of α in this case is 3.18, (left panel of Fig. 23) with 0.214 eV $\leq M_{ee} \leq$ 0.223 eV corresponding to $\Delta m^2_{32} = (2.28 - 2.46) \times 10^{-3}$ eV^2. The absolute neutrino mass scale increases for $\alpha < 1$ and decreases for $\alpha > 1$ similar to Cases 2 and 3. The behavior of α in this case is similar to Cases 2 and 3, with the lower end of α being constrained by the GERDA limit. It can also be seen from Fig. 23, that as we move towards the upper and lower ends of α, the whole 3σ range of Δm^2_{32} is not covered.

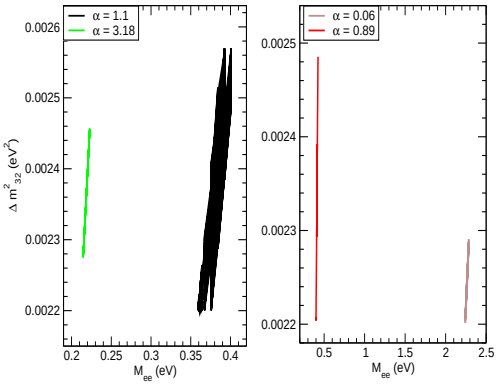

FIG. 23: The variation of Δm^2_{32} with respect to M_{ee} for Case 5 of HSMR.

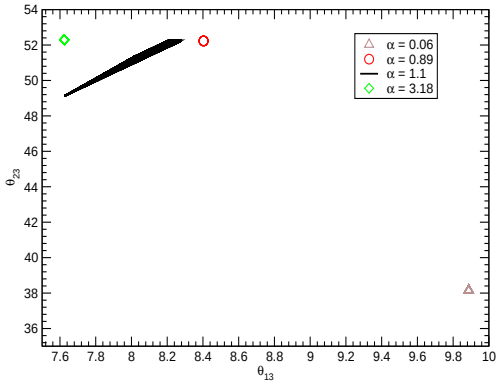

FIG. 24: The variation of θ_{23} with respect to θ_{13} for Case 5 of HSMR.

We next show the correlation of θ_{23} with respect of θ_{13} in Fig. 24. The 3σ global end point limits of θ_{23} and θ_{13}, are reached at the lowest and upper ends of α. The values of θ_{13} and θ_{23} for lowest value of $\alpha = 0.89$ are 8.40° and 52.23° respectively. These values belong to $M_{ee} = 0.4$ eV. The allowed ranges of θ_{13} and θ_{23}, at $\alpha = 1.1$ for this case are $7.62° - 8.31°$ and $49.0° - 52.3°$ respectively. The upper end of $\alpha = 3.18$, results in a global minimum value of θ_{13} and a global maximal value of θ_{23}, similar to Case 3. The lower end of α results in a global maximum value of θ_{13} and a global minimum value of θ_{23}.

We next show the variation of θ_{12} with M_{ee} in Fig. 25. The lower (30.62°) and the upper (36.81°) 3σ global limits of θ_{12}, correspond to the upper and the lowest ends of α. However, for case of $\alpha = 1.1$, the whole 3σ range of θ_{12} $(30.62° - 36.81°)$ is covered.

Finally we show in Fig. 26, the variation of the sum of the neutrino masses with respect to M_{ee}. The region with $M_{ee} \geq 0.4$ eV, for $\alpha = 0.06$, has Σm_i in the range of $6.73 - 6.85$ eV and for $\alpha = 0.89$ it is in the range $1.20 - 1.28$ eV. For $\alpha = 1.1$, with $M_{ee} < 0.4$ eV, Σm_i is in the range $1.07 - 1.22$ eV. The upper end of $\alpha = 3.18$ has the sum in the range of $0.65 - 0.67$

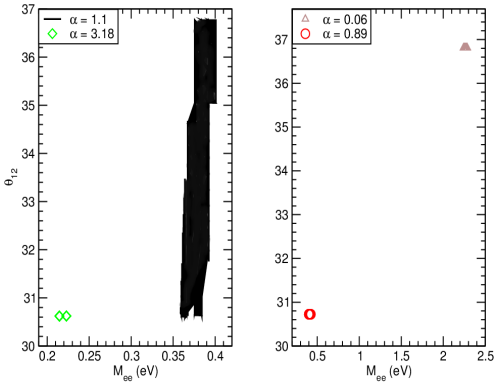

FIG. 25: The variation of θ_{12} with respect to M_{ee} for Case 5 of HSMR.

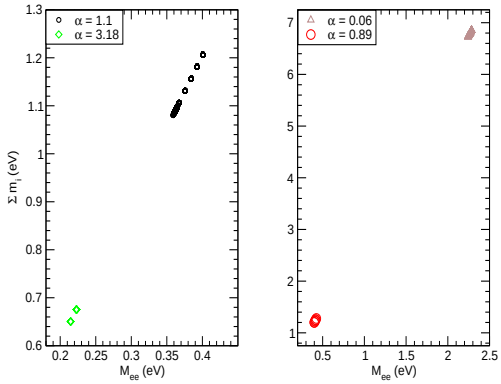

FIG. 26: The variation of Σm_i with respect to M_{ee} for Case 5 of HSMR.

eV which is remarkably lower than the previous cases. We note that the Σm_i is below the cosmological upper bound [52]. The further discussion on the cosmological constraints on our work will be provided in the last section of this paper. It is observed that Case 5 behaves almost similarly to Case 3, and is the most relaxed one in terms of M_{ee}. We can go to values of M_{ee} as low as 0.21 eV, consistent with the upper end of α. Hence, this case is partially beyond the reach of GERDA sensitivity which is maximum 0.3 eV. However, this is well within the reach of KATERIN experiment [48].

8. *Case 6:* $\theta_{12} = \alpha\ \theta^q_{12}, \quad \theta_{13} = \theta^q_{13}, \quad \theta_{23} = \alpha\ \theta^q_{23}$

We next consider the case where the leptonic mixing angle θ_{13} is identical with its CKM counterpart and the other two leptonic mixing angles are proportional to the quark mixing angles. The correlation between Δm^2_{32} and M_{ee} is shown in Fig. 27. The minimum allowed value of α, with all the mixing parameters within the global range, is 0.86. It can be seen from the left panel of Fig. 27, for this value of α, M_{ee} has a range 0.397 eV $\leq$ M_{ee} $\leq$ 0.42 eV corresponding to $\Delta m^2_{32} = (2.20 - 2.48) \times 10^{-3}$ eV^2. In case of $\alpha = 1.1$, we have 0.36 eV $\leq$ $M_{ee} \leq$ 0.424 eV which corresponds to the whole 3σ range of Δm^2_{32}. At the upper allowed value of $\alpha = 2.11$ as seen from the right panel of Fig. 27, we have 0.41 eV $\leq M_{ee} \leq$ 0.45 eV with the whole 3σ range of Δm^2_{32} covered. We have 0.64 eV $\leq M_{ee} \leq$ 0.67 eV corresponding to $\Delta m^2_{32} = (2.22 - 2.54) \times 10^{-3}$ eV^2 for the uppermost value of $\alpha = 2.19$. This end is already rejected by the GERDA limit. In this case, it is worth mentioning that the absolute

neutrino mass scale increases for both $\alpha < 1$ and $\alpha > 1$.

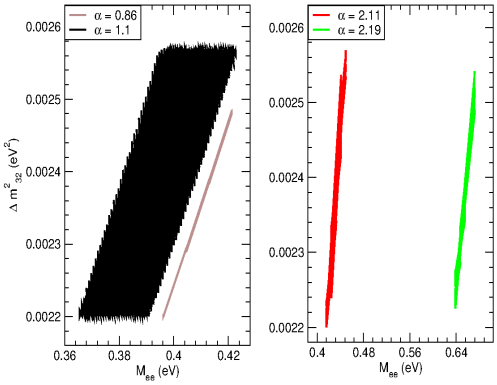

FIG. 27: The variation of Δm^2_{32} with respect to M_{ee} for Case 6 of HSMR.

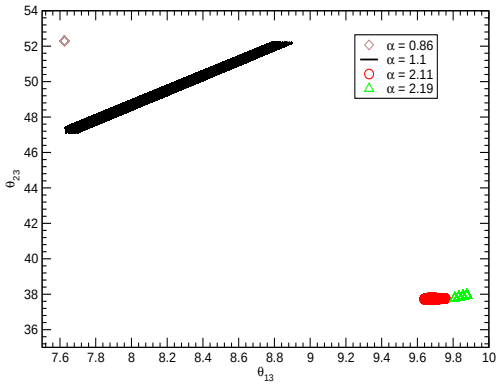

FIG. 28: The variation of θ_{23} with respect to θ_{13} for Case 6 of HSMR.

The behavior of α in this case Fig. 27 is different from Case 5, Fig. 23. Unlike Case 5 considered before, in this case for both lower and upper end values of α we get M_{ee} close to its upper limit. This is because unlike the previous cases, in this case the limit on lower value of α comes not from M_{ee} but from the neutrino oscillation parameters. Also, although the upper limit of $\alpha = 2.11$ is constrained by M_{ee} but this value is quite close to the upper limit of 2.19 obtained without the M_{ee} constraint.

In Fig. 28, we show the correlation of θ_{23} with respect of θ_{13}. The 3σ global end point limits of θ_{23} and θ_{13}, are reached at the lowest and uppermost end of α. The allowed ranges of θ_{13} and θ_{23}, at $\alpha = 1.1$ for this case are $7.62^\circ - 8.90^\circ$ and $47.0^\circ - 52.3^\circ$ respectively. At $\alpha = 2.11$, the value of θ_{13} is $9.4^\circ - 9.76^\circ$ and that of θ_{23} is $38.7^\circ - 38.8^\circ$.

We next show the variation of θ_{12} with M_{ee} in Fig. 29. The lower (30.60°) and upper (36.81°) 3σ global limits of θ_{12}, is reached at the lowest and the uppermost end of α. This behavior is quite the opposite of the behavior shown in Fig. 25 for Case 5. In case of $\alpha = 1.1$, the whole 3σ range of θ_{12} ($30.60^\circ - 36.81^\circ$) is covered. The value of θ_{12} at $\alpha = 2.11$ is $34.57^\circ - 35.02^\circ$.

Finally we show in Fig. 30, the variation of the sum of the neutrino masses with respect to M_{ee}. In case of $\alpha = 0.86$ the sum of neutrino masses Σm_i is in the range of $1.19 - 1.27$ eV. Next for $\alpha = 1.1$, Σm_i has a range of $1.1 - 1.27$ eV for $M_{ee} \leq 0.4$ eV and when $\alpha = 2.11$ it is in the range $1.26 - 1.36$ eV for 0.4 eV $\leq M_{ee} \leq 0.48$ eV.

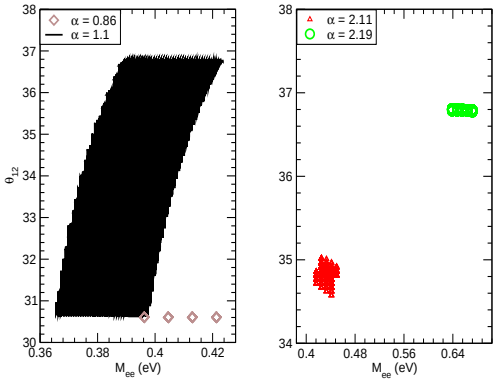

FIG. 29: The variation of θ_{12} with respect to M_{ee} for Case 6 of HSMR.

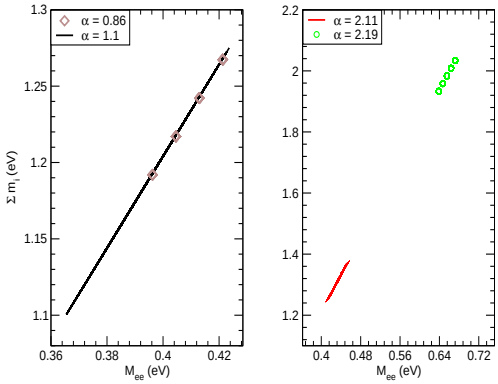

FIG. 30: The variation of Σm_i with respect to M_{ee} for Case 6 of HSMR.

9. *Case 7:* $\theta_{12} = \alpha\ \theta_{12}^q, \quad \theta_{13} = \alpha\ \theta_{13}^q, \quad \theta_{23} = \alpha\ \theta_{23}^q$

We finally consider the case where all the leptonic mixing angles are proportional to the quark mixing angle by the same proportionality constant (α). We find that the upper bound on α, is constrained by the mass limit (M_{ee}) from GERDA, whereas the lower limit on α is constrained by the 3σ global limit of the leptonic mixing angles. The lowest value of α is 0.89 and the highest value of α relaxing the GERDA limit is 2.09, whereas by taking into account the M_{ee} limit, the highest value is 2.

We next discuss the behavior of the neutrino mass and mixing parameters in Case 7, with the variation of α in the allowed range. Firstly like all the previous cases, the variation of Δm^2_{32} with M_{ee} is shown in Fig. 31. As seen from the left panel of Fig. 31, for the lowest value of $\alpha = 0.895$, we have 0.391 eV $\leq M_{ee} \leq$ 0.425 eV which corresponds to the whole 3σ global range of Δm^2_{32}. At $\alpha = 1.1$, the range of M_{ee} is 0.362 eV $\leq M_{ee} \leq$ 0.405 eV which again corresponds to the whole 3σ global range of Δm^2_{32}. The range of M_{ee} at $\alpha = 2$ is 0.4 eV $\leq M_{ee} \leq$ 0.42 eV which corresponds to the whole 3σ global range of Δm^2_{32}. The uppermost end of $\alpha = 2.09$ has 0.42 eV $\leq M_{ee} \leq$ 0.452 eV which corresponds to the whole 3σ global range of Δm^2_{32} and is rejected by the GERDA limit. Hence, the entire allowed range of α covers the whole 3σ range of m^2_{32}. The absolute neutrino mass scale increases for both $\alpha < 1$ and $\alpha > 1$ similar to Case 6. The behavior of α resembles to Case 6 with the upper and lower ends of α having values close to M_{ee}.

We show the range of θ_{23} and θ_{13} covered by the different allowed values of α in Fig. 32.

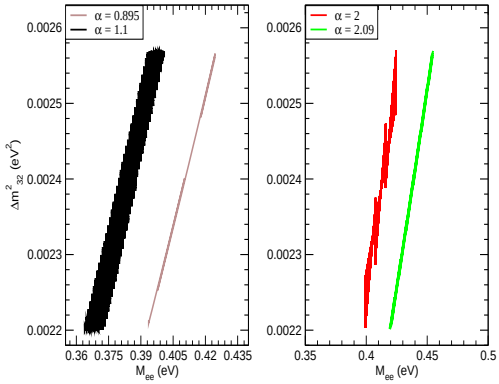

FIG. 31: The variation of Δm^2_{32} with respect to M_{ee} for Case 7 of HSMR.

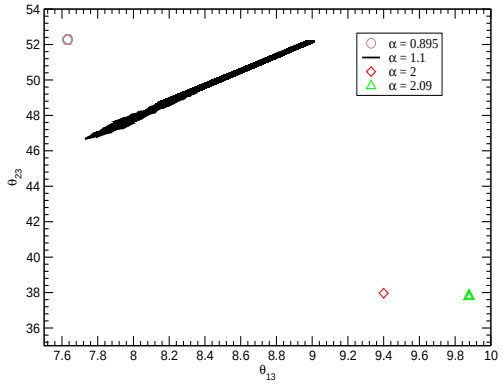

FIG. 32: The variation of θ_{23} with respect to θ_{13} for Case 7 of HSMR.

The 3σ global limits on the mixing angles are reached at the lower and uppermost ends of α. The allowed ranges of θ_{13} and θ_{23} for $\alpha = 1.1$ are $7.76^\circ - 9.02^\circ$ and $46.3^\circ - 52.26^\circ$ respectively. For $\alpha = 2.0$, the value of θ_{13} is 9.44° and that of θ_{23} is 37.8° which belongs to $M_{ee} = 0.4$ eV. The uppermost end of $\alpha = 2.09$, gives the value of θ_{13} at its global upper limit, whereas θ_{23} is kept at its global lower limit. The converse is true for the lower end of α with θ_{13}, θ_{12} at its lower value and θ_{23} at its maximum.

The variation of the third mixing angle θ_{12} with respect to M_{ee} is next plotted in Fig. 33. The pattern obtained is similar to Case 6, with the lower and upper end of α giving the 3σ global end points of θ_{12} respectively. The whole 3σ global range of θ_{12} is allowed, for $\alpha = 1.1$. The value of θ_{12} at $\alpha = 2$ is 36.6°.

Finally we plot the sum of the neutrino masses as a function of M_{ee} in Fig. 34. For $\alpha = 0.895$, range of Σm_i is $1.18 - 1.28$ eV corresponding to $0.391 \leq M_{ee} \leq 0.425$ eV. The range of Σm_i at $\alpha = 1.1$ is $1.09 - 1.18$ eV for $M_{ee} \leq 0.4$ eV. At the upper allowed value of $\alpha = 2.0$, it is $1.2 - 1.28$ eV for $0.4 \leq M_{ee} \leq 0.425$ eV. The sum of the neutrino masses is $1.27 - 1.38$ eV for $0.42 \leq M_{ee} \leq 0.452$ eV, in case of the uppermost value of $\alpha = 2.09$. This range is not allowed by the GERDA limit.

Lastly as a completion, in order to give a clear picture of all the cases discussed here along with their phenomenological consequences, we summarize our results in Table III. The upper and lower ends of α allowed by the experiments for all the cases are presented along with the corresponding values of masses and mixing angles of the neutrino sector.

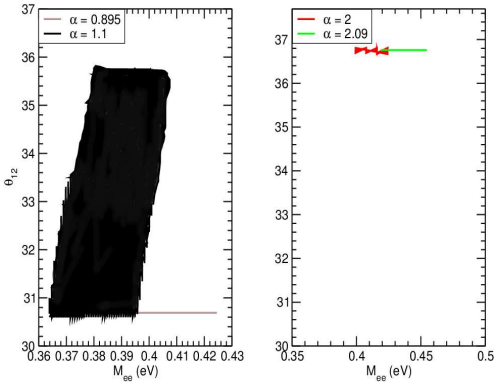

FIG. 33: The variation of θ_{12} with respect to M_{ee} for Case 7 of HSMR.

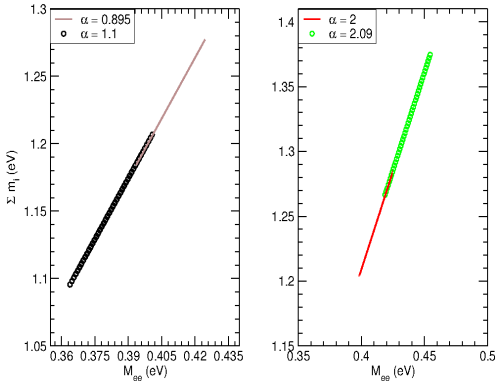

FIG. 34: The variation of Σm_i with respect to M_{ee} for Case 7 of HSMR.

10. The effects of new physics within type-I seesaw framework

In this sub-section, we discuss the possible effects of the new physics which could generate dimensional-5 operator. For sake of illustration we take type-I seesaw as the mechanism responsible for generating the effective dimensional-5 operator. The RG equations for type-I seesaw can be found in the Ref. [53]. In table IV, we show results for different cases of HSMR with a seesaw scale equals 4×10^{13} GeV which is slightly lower than the scale of the dimensional-5 operator. We have chosen this scale to demonstrate and differentiate the effects of type-I mechanism from the results obtained using dimesional-5 operator. Since the major part of RG magnification happens at scales much lower than the typical seesaw scales, the results obtained from dimension-5 operator and those obtained form type-I seesaw mechanism are not very different over a large range of parameters[28–32, 35]. Our results for type-I seesaw are as shown in Table IV. To take the effect of type-I seesaw thoroughly, we have done the RG running from the GUT scale (2×10^{16}) GeV to the seesaw scale using the full RG equation for type-I seesaw mechanism. Below the seesaw scale the right handed neutrinos are integrated out and as before, the subsequent RG running is done with effect dimension-5 operator. Here we will like to remark that since in this case the RG running is done from a higher scale i.e. GUT scale so we expect small deviations from the previous results primarily due to the larger range of RG running. The dependence of RG evolution on the chosen high scale is studied in [32, 35].

We observe from comparing Tables IV and III that for case 1 of the HSMR, the lower

	α	Masses at unification scale (eV)			Σm_i (eV)	θ_{12}°	θ_{13}°	θ_{23}°	Δm_{32}^2 (10^{-3}eV^2)	Δm_{21}^2 (10^{-5}eV^2)	M_{ee} (eV)	Lightest neutrino mass: m_1 (eV)	R
		m_1	m_2	m_3									
HSMU hypothesis	1	0.45700-0.47686	0.46-0.48	0.51573-0.53817	1.16-1.2	30.59-36.81	7.63-8.34	49-52.3	2.21-2.45	6.99-8.18	0.384-0.4	0.38397	1.5-1.8
Case 1	0.902	0.44214-0.47791	0.445-0.481	0.49891- 0.53927	1.12-1.2	30.6	7.62	52.29	2.20-2.55	6.99-8.18	0.365-0.4	0.40155	1.39-1.42
	1.28	0.47573	0.47849	0.53772	1.2	32.82	8.16	44.05	2.20	7.196	0.4	0.39968	2.1
Case 2	0.45	0.41 - 0.445	0.411 - 0.448	0.464 - 0.54	1.16-1.2	30.8	7.65	52.3	2.20-2.57	7.00-8.18	0.38-0.42	0.345-0.375	1.70-1.95
	2.5	0.415 - 0.444	0.416 - 0.445	0.468 - 0.5	1.05-1.12	31.89-36.6	7.92-9.88	37.7-48	2.20-2.53	7.00-8.18	0.342-0.378	0.348-0.373	1
Case 3	0.89	0.4771	0.4800	0.5384	1.2	30.6	8.56	52.3	2.20	6.99	0.4	0.4009	1.44
	1.52	0.3693-0.3990	0.3730-0.4030	0.4179-0.4515	0.93-1.01	30.78	7.62	52.3	2.20-2.56	6.99-8.18	0.31-0.336	0.3102-0.3352	2.16-2.21
Case 4	0.92	0.4550-0.4749	0.458-0.478	0.5135-0.5359	1.15-1.20	30.6	7.65	52.28	2.30-2.50	6.99-8.01	0.382-0.40	0.3823-0.3990	1.463-1.479
	1.67	0.4819-0.5018	0.485-0.505	0.5460-0.5685	1.22 -1.27	30.59-30.66	9.59	37.71-37.76	2.29-2.49	7.08-8.18	0.405-0.422	0.4049-0.4216	2.82-2.86
Case 5	0.89	0.475-0.505	0.478-0.508	0.536-0.570	1.20-1.28	30.72	8.40	52.23	2.20-2.48	7.00-7.97	0.4-0.42	0.399-0.424	1.465-1.485
	3.18	0.255-0.265	0.26-0.27	0.29-0.30	0.65-0.67	30.62	7.62	52.3	2.27-2.45	6.99-8.12	0.214-0.223	0.214-0.222	3.542-3.672
Case 6	0.86	0.47-0.50	0.474-0.504	0.531-0.565	1.19-1.27	30.61	7.62	52.3	2.20-2.48	6.99-8.17	0.396-0.421	0.3961-0.4211	1.241-1.268
	2.11	0.494-0.533	0.502-0.542	0.567-0.612	1.26-1.36	34.57-35.02	9.64-9.76	37.70-37.8	2.20-2.57	6.99-8.18	0.416-0.450	0.414-0.448	246.942-251.842
Case 7	0.895	0.4683-0.5051	0.4710-0.5080	0.5282-0.5696	1.185-1.22	30.68	7.63	52.28	2.20-2.31	6.99-8.18	0.393-0.4	0.3935-0.4044	1.34-1.37
	2	0.4738	0.4800	0.5413	1.18	36.6	9.44	37.8	2.20	7.248	0.39	0.3977	81.7-82.11

TABLE III: The allowed predictions for HSMU and the different cases of the HSMR for lower and upper allowed values of α, Eqs. (14-20).

allowed end of α effectively does not change. As expected, there are slight changes in the value of the observables. For example, the M_{ee} decreases and reaches to the value 0.349 eV compare to the prediction given in table III. Similar observation for the mass of the lightest neutrino. The upper end of α changes after introducing seesaw scale, primarily due to increased RG running range. In Table III, the upper allowed end for case 1 is 1.28. As we observe in Table IV, it is now 1.71 and parameter space is bit expanded. However, there is no significant qualitative change in our results which are same as before.

Similarly, for case 2, one can observe from the Tables IV and III that the lower end of α does not change much. The results are stable and similar to Table III. The upper end of α changes slightly and is 2.59 now. Again as before, there is no significant qualitative change in our results which are same as before.

In case 3 of Table IV, the lower value of α has shifted a bit from that of TableIII, that is from 0.89 to 0.75, but the higher value remains intact being 1.52. The parameters also

cover more or less the same span as before and show a stable situation .

The observed pattern in case 4 is same as the case 1, as we see that the lower end does not change while the upper end changes from 1.67 to 1.76 after the inclusion of type-I seesaw (see Table IV and Table III for comparison). The value of M_{ee} and the mass of lightest neutrino decreases compare to the values given in Table III and attain the values 0.3508 eV and 0.3506 eV, respectively.

The observed pattern in case 5 is also same as that obtained in Table III. Comparing the results with Table III, we find that the value of α at the lower end changes slightly. The lower end saturates the bound for M_{ee}, whereas at the upper end the value of M_{ee} turns out to be 0.205 eV, which is slightly smaller than the value quoted in Table III.

In case 6, the upper value of α changes very slightly compared to Table III, whereas the lower value remains the same. In this case both the lower and upper end saturates the bound for M_{ee}.

As expected, the results for case 7 are stable as can be observed from Tables III and IV, where the lower end of α is now 0.896 instead of 0.895 and the higher end remains the same, namely $\alpha = 2$.

Thus, as expected the results obtained with the framework of type-I seesaw mechanism are qualitatively same as those obtained using only dimension-5 effective operator. The general observation is that the absolute mass scale is decreasing due to the RG evolution starting from GUT scale (2×10^{16} GeV) which is higher than the scale of dimensional-5 operator. This leads to a slight change in the allowed end of α that is constrained by the observable M_{ee}. That is why, we observe a slight change in the values of mixing angles. We remark that if the high scale from where RG evolution begins, is chosen to be 10^{14} GeV with a seesaw scale equals 4×10^{13} GeV, we recover the results obtained with dimensional-5 operator which is naturally expected.

V. THEORETICAL MODELS FOR HIGH SCALE MIXING RELATIONS

In this section, we address the theoretical implementation of HSMR hypothesis from the model building point of view. The only aim of this section is to illustrate that the HMSR hypothesis can be simply realized in models based on flavor symmetries. We follow the same line of argument as presented in Ref. [28].

	α	Masses at unification scale (eV)			Σm_i (eV)	θ_{12}°	θ_{13}°	θ_{23}°	Δm_{32}^2 (10^{-3}eV^2)	Δm_{21}^2 (10^{-5}eV^2)	M_{ee} (eV)	Lightest neutrino mass: m_1 (eV)	R
		m_1	m_2	m_3									
Case 1	0.903	0.46547	0.469	0.53833	1.04	31.06	7.63	52.30	2.209	8.00	0.349	0.34419	1.48
	1.71	0.54038-0.54199	0.545-0.546	0.62793-0.62968	1.203- 1.205	30.82 - 33.38	8.68 - 9.87	37.75 - 40.25	2.201-2.26	7.05-7.96	0.399-0.4	0.39815	4.89
Case 2	0.47	0.486067-0.486077	0.49	0.56241 - 0.562434	1.08-1.0821	30.66-30.92	7.62	52.15-52.19	2.2-2.23	7.65-8	0.359	0.359022-0.359308	1.96-1.99
	2.59	0.478-0.480	0.481- 0.483	0.55 - 0.554	1.06	30.68-31.2	9.1-9.16	42.96-43.51	2.5-2.56	7-7.24	0.354	0.353-0.354	1
Case 3	0.75	0.541797 - 0.542934	0.545 - 0.546	0.625782 - 0.627092	1.20171 - 1.20407	30.6074 - 32.7328	8.74619 - 8.95191	51.3341 - 52.2853	2.2-2.24	6.99-8.16	0.399 - 0.4	0.399 - 0.4	1.351 - 1.374
	1.52	0.392477	0.3971	0.455448	0.879869	30.7133	7.63895	52.2976	2.28	7.05	0.291584	0.291263	2.52
Case 4	0.92	0.4744	0.478	0.5487	1.06	30.98	7.64	52.27	2.266	8.081	0.3508	0.3506	1.55
	1.76	0.5484-0.5544	0.552-0.558	0.6366-0.6435	1.22-1.23	36.09-36.55	9.80-9.87	37.71-37.83	2.204-2.207	7.101-7.837	0.4045-0.4088	0.4039-0.4083	4.7-4.85
Case 5	0.80	0.537	0.540	0.621	1.191	32.68	7.79	49.17	2.20	8.09	0.396	0.396	1.532
	3.18	0.274	0.280	0.321	0.623	30.65	7.63	52.3	2.45	7.22	0.205	0.205	4.582
Case 6	0.86	0.497	0.500	0.574	1.104	31.09	7.62	52.3	2.20	7.86	0.367	0.367	1.301
	2.14	0.544	0.555	0.642	1.22	35.06	9.88	37.77	2.21	8.18	0.402	0.400	957
Case 7	0.896	0.49	0.50	0.57	1.104	30.65 - 31.41	7.62	52.26	2.24	7.1-8.1	0.36	0.36	1.42
	2	0.5	0.49-0.51	0.58	1.12	34.30 - 36.69	9.52 - 9.84	37.80 - 38.07	2.28 - 2.47	7.08 - 7.21	0.37	0.37	155.5

TABLE IV: The allowed predictions for the different cases of the HSMR for lower and upper allowed values of α, Eqs. (14-20) within the framework of type-I seesaw for sea-saw scale 4×10^{13} GeV. It should be noted that RG evolution begins from GUT scale which is 2×10^{16} GeV.

Now we discuss a simple realization of HSMR relations using abelian Z_7 flavor symmetry. To realize the HSMR relations we add three $SU(2)$ triplet scalars ξ_i; $i = 1, 2, 3$ to the particle content of MSSM. The smallness of neutrino masses can then be explained by the type-II seesaw mechanism. Let the quarks and leptons and scalars transform under Z_7 as follows

$$\begin{aligned} Q_L^1 \sim 1, \quad Q_L^2 \sim \omega, \quad Q_L^3 \sim \omega^3, \quad u_R, d_R \sim 1, \quad c_R, s_R \sim \omega, \quad t_R, b_R \sim \omega^3 \\ L_L^1 \sim 1, \quad L_L^2 \sim \omega, \quad L_L^3 \sim \omega^3, \quad e_R \sim 1, \quad \mu_R \sim \omega, \quad \tau_R \sim \omega^3 \\ H_u, H_d \sim 1, \quad \xi_1 \sim 1, \quad \xi_2 \sim \omega^2, \quad \xi_3 \sim \omega^6 \end{aligned} \tag{46}$$

where $\omega = e^{\frac{2\pi i}{7}}$ is the seventh root of unity. In the above equation Q_L^i, L_L^i; $i = 1, 2, 3$ are the quark and the lepton doublets respectively whereas u_R, d_R, c_R, s_R, $t_R, b_R, e_R, \mu_R, \tau_R$ are the quark and the charged lepton singlets. Moreover, H_u, H_d are the two scalar doublets required to give mass to the up and down type quarks respectively.

It is easy to see from Eq. (46) that the Z_7 symmetry leads to diagonal mass matrices for both the quarks and the leptons leading to $U_{CKM} = U_{PMNS} = I$. To obtain the realistic

CKM and PMNS matrices as well as the HSMR relations, we allow for small Z_7 symmetry breaking terms as done in Ref. [54] albeit for A_4 symmetry. Such corrections can arise from soft supersymmetry breaking sector as shown in Ref. [55–57]. Allowing for symmetry breaking terms of the form $|h_i'''| << |h_i''| << |h_i'| << |h_i|$ where h_i are the terms invariant under Z_7 symmetry and h_i', h_i'' and h_i''' are the symmetry breaking terms transforming as ω, ω^2 and ω^3 respectively under Z_7 symmetry. Following the approach of Ref. [54] one can then easily realize the HSMR relations. Here we want to emphasize that owing to quite different masses of quarks and charged leptons, this analysis will in general lead to HSMR relations and not to HSMU relations. To obtain HSMU relations from such an approach one has to invoke a symmetry or mechanism to ensure that the symmetry breaking terms are exactly same in both quark and lepton sectors.

Before, ending this section we would like to further remark that although we have only discussed realization of HSMR relations through the Z_7 symmetry, they can also be quite easily and naturally realized using other flavor symmetries and also using other type of seesaw mechanisms. For example, one can also realize HSMR relations within the framework of type-I seesaw mechanism using Z_7 symmetry. For this, instead of adding triplet scalars we add three right handed neutrinos which transform as $N_{1R} \sim 1, N_{2R} \sim \omega, N_{3R} \sim \omega^3$ under the Z_7 symmetry. We also add three heavy singlet scalars ϕ_i; $i = 1, 2, 3$ transforming as $\phi_i \sim 1, \phi_2 \sim \omega^5, \phi_3 \sim \omega$ under Z_7 symmetry. Following computations analogous to those done above, one can again easily obtain the HSMR relations. Thus, it is clear that HSMR relations are very natural and can be easily realized using discreet flavor symmetries. In this work we do a model independent analysis of the consequences of the HSMR relations assuming they are realized at the high scale by appropriate flavor symmetries.

VI. SUMMARY

The very small mass of the neutrinos along with a large mixing among them is arguably a remarkable observation. This phenomenon is starkly different from the mixing in the quark sector which is small in the SM. The quest to understand the origin of a large mixing among the neutrinos and a small mixing among the quarks has led to many interesting theoretical ideas. Many beyond the standard model scenarios have been constructed, trying to understand the major theoretical challenge posed by the neutrino mixing. GUT theories

with the quark-lepton unification have been extensively used in the literature to understand the neutrino sector at low energies. The postulated HSMR in this work is another effort to understand this extraordinary observation of neutrino mixing. We have shown from a model building point of view, how the HSMR can be naturally realized using different flavor symmetries and seesaw mechanisms. We have first considered the most general relation among the leptonic and the quark mixing angles, with different proportionality constants (α_i). We then list the different possible cases which arise, for the maximum and minimum allowed values of α_i. It is found that for the allowed range of α_i, M_{ee} is between 0.35 eV - 0.4 eV. The future experiments from GERDA will severely constrain these scenarios. We then look into more simplified cases to have a clear physical picture and therefore consider the α_i to be equal for the three generations and vary k_i to 0 or 1. We then list the seven possible ways the quark and the leptonic mixing angles can be proportional to each other (cf. Eqs. (14- 20)). It is remarkable that these relations naturally explain the difference between V_{CKM} and U_{PMNS} at the low scale. Furthermore, the QLC relation and the observation in Eq. (2) can be easily recovered by these relations.

We have thoroughly investigated the implications and the phenomenological consequences of all the possible cases, taking into account the latest experimental constraints. The whole analysis has been done with the assumption of normal hierarchy and QD mass pattern. In general, we have discovered three new correlations among Δm^2_{32}, M_{ee}, θ_{12} and sum of neutrino masses. These correlations are not investigated in previous studies.

We first discuss about the HSMU scenario, which is a special case of all the HSMR scenarios in the α =1 limit. The behavior of the neutrino masses and the mixing parameters at the low energy scale is discussed in detail for all the cases in HSMR with the value of α deviating from unity in the allowed range. The allowed range of α is bounded by the recent experimental results listed in Table I and the upper limit on M_{ee} provided by GERDA [51]. It is seen that for all the cases except Case 2, the M_{ee} constraint from the GERDA results in either upper (Cases 1, 4, 6 and 7) or lower (Cases 3 and 5) limit of α. Otherwise the allowed value of α is mostly constrained by the 3σ global limits on neutrino mixing parameters.

An interesting feature is observed in Case 2, where the lower end is constrained by the 3σ global limits of neutrino mixing parameters but the upper end is constrained by the value of the ratio R, which contributes through threshold corrections. We have worked here in the inverted hierarchy scheme in the charged slepton sector, forcing the ratio to be either greater

than or equal to one. A common behavior has been observed for all the cases, where we always find a strong correlation between θ_{23} and θ_{13}, for all the allowed values of α except at the end points which corresponds to a point in the $\theta_{23} - \theta_{13}$ plane. It is also seen that among all the experimental constraints M_{ee} is the most interesting one as it mostly constrains the different cases as well as differentiates among them. If in the future the upper limit from GERDA goes down to 0.35 eV, then HSMU, Case 1, Case 4, Case 6 and Case 7 will be ruled out. The ones who will survive will be Cases 2, 3 and 5 which allows M_{ee} as low as 0.2 eV but with the value of $\alpha > 1$. The constraint on M_{ee} can automatically be reverted to the sum of the neutrino masses. It will show a similar behavior while discriminating the various cases. We also notice that if we take into account the GERDA limit of 0.4 eV, then the allowed range of α in Cases 1, 3 and 5 is limited to a small region in the $\theta_{23} - \theta_{13}$ plane (Figs. 8, 16, 24). Therefore these cases along with HSMU will be ruled out, if the best fit value of θ_{23} becomes less than 44° or that of θ_{13} becomes greater than 8.55° in the future. We further see that Cases 2 and 5 can survive longer, and the region of $M_{ee} = 0.2$ eV is beyond the sensitivity of GERDA which is maximun 0.3 eV. The region of $M_{ee} = 0.2$ eV will easily be probed by KATRIN[48] since m_β is approximately identical to M_{ee} in this work. Here, we pause to comment on the cosmological limit on the sum of the neutrino masses [52]. Our predictions in all cases except Case 5 are slightly above the upper cosmological bound of 0.72 eV. As commented earlier, this bound is model dependent. Hence, it is preferred to test predictions of this work in a laboratory based experiment, like GERDA [51].

We also observe that Cases 3 and 5 show similar behavior, this is mainly because both consider the framework, where the neutrino mixing angle θ_{23} is equal to the quark mixing angle by a proportionality constant $\alpha\theta^q_{23}$. Although Case 5 also has the condition of $\theta_{13} = \alpha\ \theta^q_{13}$, but at the GUT scale $\theta^q_{13} \ll \theta^q_{23}$, therefore the effect of θ^q_{23} dominates. The same pattern can be observed for Case 1 and Case 4, explained through the same argument, $\theta^q_{13} \ll \theta^q_{12}$ at the GUT scale. Continuing the same argument as expected we find that Case 7 displays similar behavior as Case 6. The effect of the neutrino mixing angle θ_{13} being proportional to the quark mixing has many interesting results, as it leads to the most optimistic case. However once the other angles become proportional, this effect is subdued. Finally we note that all these interpretations have been done with the assumption that the Dirac and the Majorana phases of the PMNS matrix are zero and phenomenological consequences can change with nonzero phases. The overall scenario depicting a quark-lepton symmetry at a

high scale through HSMR can be narrowed down to a particular case or completely ruled out, only from the future improved experimental constraints. These constraints can be from the neutrinoless double beta decay [51], or the LHC constraints on the SUSY spectrum.

The different scenarios of the HSMR can be discriminated through measurement of various observables like M_{ee} and by precise determination of the values of the mixing angles, particularly θ_{13} and θ_{23} mixing angles. As we have shown in the figures for various cases as well in the tables, the allowed ranges for M_{ee} and the angles are different for different cases and a precise determination of these observables can be used as a way to distinguish various cases of HSMR. In addition to neutrino observables one can also use other process like lepton-flavor violation to distinguish the different allowed cases. The mass-splitting in the charged-slepton sector is given by the ratio $R = \frac{M_{\tilde{e}}}{M_{\tilde{\mu},\tilde{\tau}}}$. We observe from tables II and III that the ratio R almost discriminate every scenario. Hence the processes like $\mu \to e\gamma$, $\mu \to eee$ and anomalous magnetic moment of the electron. For example, the SUSY contribution to the anomalous magnetic moment of the electron directly depends on the ratio R [58]. The detail study of this aspect of the work is not possible in this paper.

Furthermore, for sake of completion, we also present our results in the framework of the type-I seesaw. The aim is to show how the predictions do not change in any significant way and that the analysis done with effective dimension-5 operator is quite robust. As argued before, this is not surprising as the major part of RG magnification happens only at much lower scales closer to SUSY breaking scale. At such low scales, the effective dimension-5 operator provides a very good approximation to the high scale seesaw mechanisms. The mass scale of the right-handed neutrinos is chosen 4×10^{13} GeV which is close to the scale of the dimensional-5 operator. We notice that parameter spcae increases very slowly as we decrease the scale of new physics primarily due to increased span of RG running. However predictions do not change in any significant manner and are quite robust.

We also comment on a general theoretical view which is more general than the HSMU hypothesis and the HSMR. Assuming that at some high scale, both the mixing matrices (CKM and PMNS) are approximately unit matrices, but some perturbation can mix the generations leading to the Wolfenstein form of the mixing in both the quark and lepton sectors. This results in the mixing between the first and the second generations to be λ (a small number of order 0.2), the second and the third generations mixing to be second order in λ i.e. $\sin\theta_{23} \sim \lambda^2$ while the first and the third generations mixing to be third order order

in λ i.e. $\sin\theta_{13} \sim \lambda^3$. Now after RG evolution the CKM mixing angles do not change much but the PMNS mixing angles are dramatically magnified for the reasons already mentioned in this as well as our earlier papers [32–34].

Finally, in short, crux of our paper is following.

- We have proposed and studied the HSMR hypothesis which is a more general framework than the HSMU hypothesis.

- The HSMR hypothesis provides a very simple explanation of the observed large neutrino mixing. The present and future neutrino experiments can easily test predictions of our work. If our predictions are confirmed by experiments, like GERDA, it would be a good hint of quark-lepton unification at high scale.

- We observe that the HSMU hypothesis represents $\alpha = 1$ limit of the HSMR hypothesis and is constrained by the lowest allowed value of M_{ee} which is 0.384 MeV. Therefore, if the HSMU hypothesis is ruled out by experiments, like GERDA, the other HSMR cases with $\alpha \neq 1$ may survive and their confirmation would be itself a strong hint of the proportinality between quark and leptonic mixing angles which is the basis of the HSMR hypothesis.

- We have done a rigorous, thorough and comprehensive study with the HSMR hypothesis which does not exist in the literature. All results reported in the literature using the HSMU hypothesis, are very small subset of our results with the HSMR hypothesis presented in our paper. Moreover, we have also thoroughly compared HSMR hypothesis with respect to the HSMU.

- In our work, we have discovered new strong correlations among different experimental observables for every limit of the HSMR hypthesis. These correlations do not exist in the literature and are easily testable in present ongoing experiments. For example, there is a strong correlation between Δm^2_{32} and M_{ee}. This correlation can be easily tested by GERDA experiment. There are two more such correlations namely among θ_{12}, M_{ee}, Σm_i and M_{ee} discussed in our work which are completely new and unexplored in the literature.

- Furthermore, we have comprehensively studied a strong correlation between θ_{23} and θ_{13} and predictions can be easily tested in present ongoing experiments. This correlation

was studied in a previous study in a specific limit. Since we have done a comprehensive full parameter scan, this correlation has become a robust band now.

Acknowledgments

It is a pleasure to thank Antonio Pich for his valuable suggestions and comments on the manuscript. GA dedicates this paper to I. Sentitemsu Imsong. The work of GA has been supported in part by the Spanish Government and ERDF funds from the EU Commission [Grants No. FPA2011-23778, FPA2014-53631-C2-1-P No. and CSD2007-00042 (Consolider Project CPAN)]. The work of SG is supported by Conselho Nacional de Desenvolvimento Científico e Tecnológico (CNPq) Brazil grant 151112/2014-2.

[1] F. Capozzi, G. L. Fogli, E. Lisi, A. Marrone, D. Montanino and A. Palazzo, Phys. Rev. D **89** (2014) 9, 093018 [arXiv:1312.2878 [hep-ph]].

[2] M. C. Gonzalez-Garcia, M. Maltoni and T. Schwetz, JHEP **1411** (2014) 052 [arXiv:1409.5439 [hep-ph]].

[3] D. V. Forero, M. Tortola and J. W. F. Valle, Phys. Rev. D **90** (2014) 9, 093006 [arXiv:1405.7540 [hep-ph]].

[4] H. Ishimori, T. Kobayashi, H. Ohki, Y. Shimizu, H. Okada and M. Tanimoto, Prog. Theor. Phys. Suppl. **183** (2010) 1 [arXiv:1003.3552 [hep-th]].

[5] W. Grimus and P. O. Ludl, J. Phys. A **45** (2012) 233001 [arXiv:1110.6376 [hep-ph]].

[6] G. Altarelli and F. Feruglio, Rev. Mod. Phys. **82** (2010) 2701 [arXiv:1002.0211 [hep-ph]].

[7] S. F. King and C. Luhn, Rept. Prog. Phys. **76** (2013) 056201 [arXiv:1301.1340 [hep-ph]].

[8] E. Ma and R. Srivastava, Phys. Lett. B **741** (2015) 217 [arXiv:1411.5042 [hep-ph]].

[9] E. Ma and R. Srivastava, Mod. Phys. Lett. A **30** (2015) 26, 1530020 [arXiv:1504.00111 [hep-ph]].

[10] M. Holthausen and K. S. Lim, Phys. Rev. D **88** (2013) 033018 [arXiv:1306.4356 [hep-ph]].

[11] T. Araki, H. Ishida, H. Ishimori, T. Kobayashi and A. Ogasahara, Phys. Rev. D **88** (2013) 096002 [arXiv:1309.4217 [hep-ph]].

[12] H. Ishimori and S. F. King, Phys. Lett. B **735** (2014) 33 [arXiv:1403.4395 [hep-ph]].

[13] C. S. Lam, Phys. Rev. D **89** (2014) 9, 095017 [arXiv:1403.7835 [hep-ph]].

[14] J. C. Pati and A. Salam, Phys. Rev. D **10** (1974) 275 [Erratum-ibid. D **11** (1975) 703].

[15] H. Georgi and S. L. Glashow, Phys. Rev. Lett. **32** (1974) 438.

[16] H. Fritzsch and P. Minkowski, Annals Phys. **93** (1975) 193.

[17] A. Y. Smirnov, hep-ph/0402264.

[18] M. Raidal, Phys. Rev. Lett. **93** (2004) 161801 [hep-ph/0404046].

[19] H. Minakata and A. Y. Smirnov, Phys. Rev. D **70** (2004) 073009 [hep-ph/0405088].

[20] P. H. Frampton and R. N. Mohapatra, JHEP **0501** (2005) 025 [hep-ph/0407139].

[21] S. K. Kang, C. S. Kim and J. Lee, Phys. Lett. B **619** (2005) 129 [hep-ph/0501029].

[22] K. Abe *et al.* [T2K Collaboration], Phys. Rev. Lett. **107** (2011) 041801 [arXiv:1106.2822 [hep-ex]].

[23] P. Adamson *et al.* [MINOS Collaboration], Phys. Rev. Lett. **107** (2011) 181802 [arXiv:1108.0015 [hep-ex]].

[24] Y. Abe *et al.* [Double Chooz Collaboration], Phys. Rev. D **86** (2012) 052008 [arXiv:1207.6632 [hep-ex]].

[25] J. K. Ahn *et al.* [RENO Collaboration], Phys. Rev. Lett. **108** (2012) 191802 [arXiv:1204.0626 [hep-ex]].

[26] F. P. An *et al.* [Daya Bay Collaboration], Phys. Rev. Lett. **108** (2012) 171803 [arXiv:1203.1669 [hep-ex]].

[27] S. Antusch, C. Gross, V. Maurer and C. Sluka, Nucl. Phys. B **866** (2013) 255 [arXiv:1205.1051 [hep-ph]].

[28] R. N. Mohapatra, M. K. Parida and G. Rajasekaran, Phys. Rev. D **69** (2004) 053007 [hep-ph/0301234].

[29] R. N. Mohapatra, M. K. Parida and G. Rajasekaran, Phys. Rev. D **71** (2005) 057301 [hep-ph/0501275].

[30] R. N. Mohapatra, M. K. Parida and G. Rajasekaran, Phys. Rev. D **72** (2005) 013002 [hep-ph/0504236].

[31] S. K. Agarwalla, M. K. Parida, R. N. Mohapatra and G. Rajasekaran, Phys. Rev. D **75** (2007) 033007 [hep-ph/0611225].

[32] G. Abbas, S. Gupta, G. Rajasekaran and R. Srivastava, Phys. Rev. D **89** (2014) 9, 093009 [arXiv:1401.3399 [hep-ph]].

[33] G. Abbas, S. Gupta, G. Rajasekaran and R. Srivastava, Manuscript under preparation

[34] R. Srivastava, arXiv:1503.07964 [hep-ph].

[35] G. Abbas, S. Gupta, G. Rajasekaran and R. Srivastava, arXiv:1312.7384 [hep-ph].

[36] S. Antusch, J. Kersten, M. Lindner and M. Ratz, Nucl. Phys. B **674** (2003) 401 [hep-ph/0305273].

[37] P. H. Chankowski and Z. Pluciennik, Phys. Lett. B **316** (1993) 312 [hep-ph/9306333].

[38] K. S. Babu, C. N. Leung and J. T. Pantaleone, Phys. Lett. B **319** (1993) 191 [hep-ph/9309223].

[39] S. Antusch, M. Drees, J. Kersten, M. Lindner and M. Ratz, Phys. Lett. B **519** (2001) 238 [hep-ph/0108005].

[40] S. Antusch, M. Drees, J. Kersten, M. Lindner and M. Ratz, Phys. Lett. B **525** (2002) 130 [hep-ph/0110366].

[41] E. J. Chun and S. Pokorski, Phys. Rev. D **62** (2000) 053001 [hep-ph/9912210].

[42] P. H. Chankowski, A. Ioannisian, S. Pokorski and J. W. F. Valle, Phys. Rev. Lett. **86** (2001) 3488 [hep-ph/0011150].

[43] E. J. Chun, Phys. Lett. B **505** (2001) 155 [hep-ph/0101170].

[44] P. H. Chankowski and P. Wasowicz, Eur. Phys. J. C **23** (2002) 249 [hep-ph/0110237].

[45] N. Craig, arXiv:1309.0528 [hep-ph].

[46] C. Kraus, B. Bornschein, L. Bornschein, J. Bonn, B. Flatt, A. Kovalik, B. Ostrick and E. W. Otten *et al.*, Eur. Phys. J. C **40** (2005) 447 [hep-ex/0412056].

[47] V. N. Aseev *et al.* [Troitsk Collaboration], Phys. Rev. D **84** (2011) 112003 [arXiv:1108.5034 [hep-ex]].

[48] G. Drexlin, V. Hannen, S. Mertens and C. Weinheimer, Adv. High Energy Phys. **2013** (2013) 293986 [arXiv:1307.0101 [physics.ins-det]].

[49] W. Rodejohann, J. Phys. G **39** (2012) 124008 [arXiv:1206.2560 [hep-ph]].

[50] S. M. Bilenky and C. Giunti, Int. J. Mod. Phys. A **30** (2015) 04n05, 1530001 [arXiv:1411.4791 [hep-ph]].

[51] M. Agostini *et al.* [GERDA Collaboration], Phys. Rev. Lett. **111** (2013) 12, 122503 [arXiv:1307.4720 [nucl-ex]].

[52] P. A. R. Ade *et al.* [Planck Collaboration], arXiv:1502.01589 [astro-ph.CO].

[53] S. Antusch, J. Kersten, M. Lindner, M. Ratz and M. A. Schmidt, JHEP **0503** (2005) 024 [hep-ph/0501272].

[54] E. Ma, Mod. Phys. Lett. A **17**, 627 (2002) [hep-ph/0203238].

[55] K. S. Babu, E. Ma and J. W. F. Valle, Phys. Lett. B **552**, 207 (2003) [hep-ph/0206292].

[56] K. S. Babu, B. Dutta and R. N. Mohapatra, Phys. Rev. D **60**, 095004 (1999) [hep-ph/9812421].

[57] F. Gabbiani, E. Gabrielli, A. Masiero and L. Silvestrini, Nucl. Phys. B **477**, 321 (1996) [hep-ph/9604387].

[58] D. Stockinger, J. Phys. G **34**, R45 (2007) doi:10.1088/0954-3899/34/2/R01 [hep-ph/0609168].